3-D SAM

Part 2

Nanoparticles - spontaneous ordering

when monodispersed....

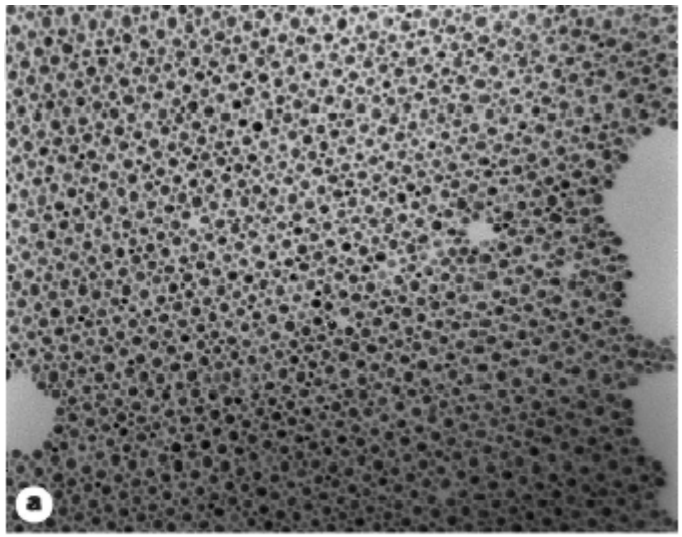

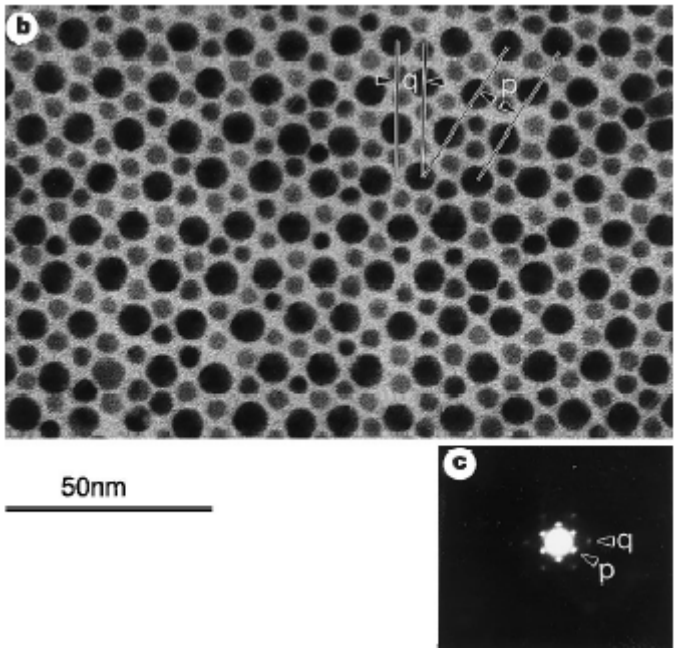

An ordered raft comprising Au nanoparticles of two distinct sizes with R_B/R_A < 0:58. Shown are electron micrographs at low (a) and higher (b) magnification. c, The low-angle superlattice electron diffraction pattern obtained from this bimodal raft structure.

C. J. Kiely, J. Fink,M. Brust, D. Bethell, D. J. Schiffrin, Nature, **1998**, 396, 444.

3D alkanethiolate monolayers

Scheme 1. A Schematic 2D Representation of the RS/Au Nanoparticle Packing Structure in the Solid State[a]

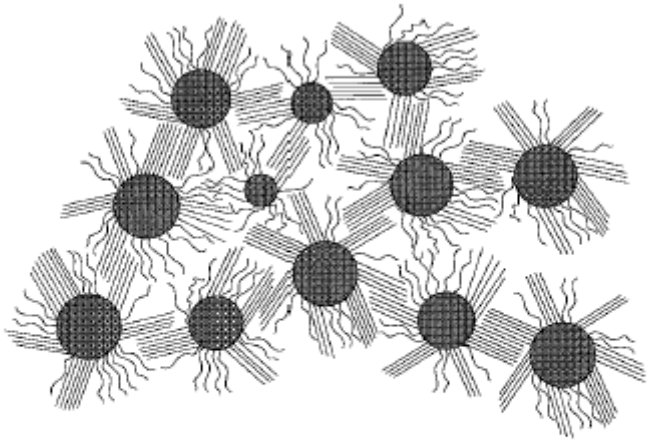

[a] In this description, *domains* or *bundles* of ordered alkylthiolate chains on a given Au particle will interdigitate into the chain domains of neighboring particles in order to compensate for the substantial decrease in the chain density which occurs toward the methyl chain end. Chains with large populations of *gauche* bonds may arise from (i) those which occupy interstitial regions in the particle lattice and cannot efficiently overlap with adjacent chains or from (ii) chains residing at domain boundaries.

Scheme 2. The Types of Chain Dynamic Processes Suggested by the ^{2}H NMR Line Shapes of the Deuterated $C_{18}S$/Au Nanoparticles[a]

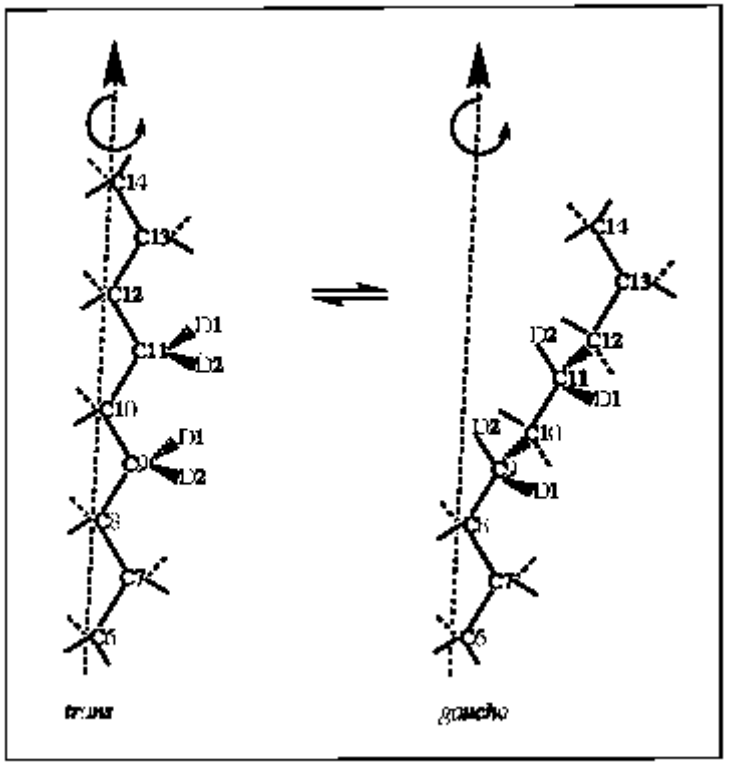

[a] These processes involve *trans-gauche* bond isomerization and pseudorotational motion of individual chain segments about the long axis of the alkanethiolate molecule.

A. Badia, L. Cuccia, L. Demers, F. Morin, B. R. Lennox, J. Am. Chem. Soc., **1997**, 119, 2682.

3D alkanethiolate monolayers

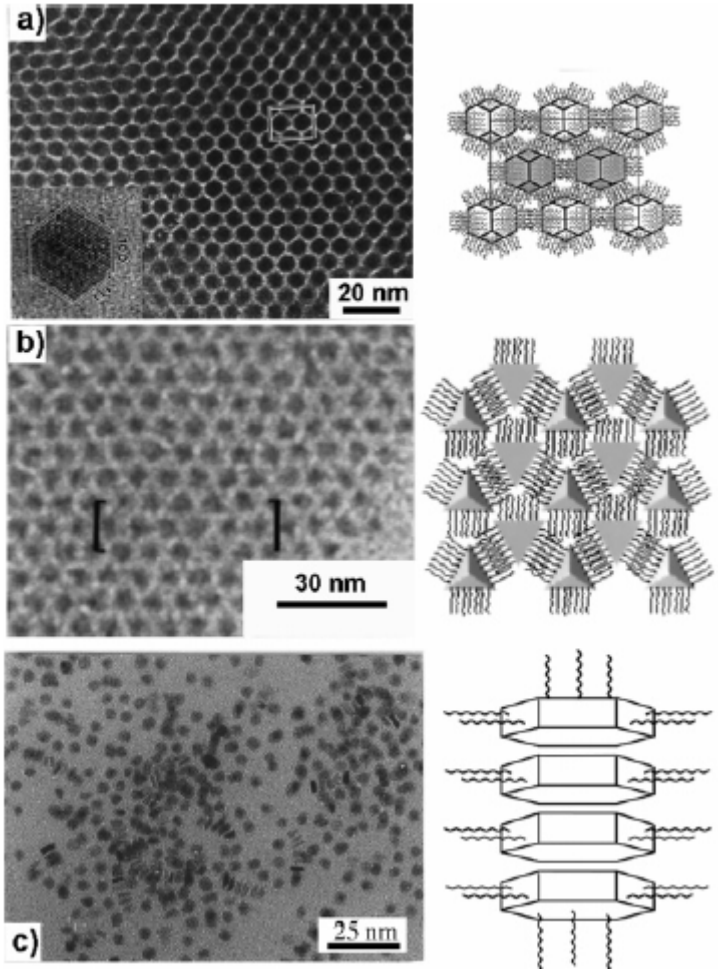

Figure 11. (a) (Left) TEM image of a face-centered, cubicpacked, array of silver nanoparticles, passivated with a dodecanethiolate monolayer, with a truncated octahedral morphology (see inset). (Right) Representation of the proposed packing of the particles via interdigitation of the bundled alkyl chains on each face. (b) (Left) TEM image of a monolayer of self-assembled silver tetrahedra passivated with dodecanethiolates. The bracketed area most closely matches the proposed model.

Langmuir **1998**, *14*, 17−30

Alkanethiolate Gold Cluster Molecules with Core Diameters from 1.5 to 5.2 nm: Core and Monolayer Properties as a Function of Core Size

Michael J. Hostetler,[†] Julia E. Wingate,[†] Chuan-Jian Zhong,[‡] Jay E. Harris,[†] Richard W. Vachet,[†] Michael R. Clark,[†] J. David Londono,[§] Stephen J. Green,[†] Jennifer J. Stokes,[†] George D. Wignall,[§] Gary L. Glish,[†] Marc D. Porter,[‡] Neal D. Evans,[∥] and Royce W. Murray*,[†]

Table 1. Size and Composition Results for Different Cluster Preparations

preparation conditions[a]	SAXS[b] R_G, nm, max/min	SAXS[c] R_{POROD}, nm	HRTEM[d] R_{TEM}, nm	TGA[e] % organic	NMR[f] CH_3, ν_{FWHM} Hz
−78°,2X,sd	1.7/0.91	0.76	—	30.7	16
0°,2X,fd	—	—	1.1	28.8	21
0°,2X,md	—	—	—	26.7	22.5
0°,2X,sd	1.7/1.0	0.89	1.1	26.2	25.5
RT,1X,fd	1.7/1.2	1.0	—	25.6	24.5
RT,4X,fd	1.7/1.1	0.94	—	24.9	26
RT,2X,sd	1.6/1.2	0.96	—	24.5	27
RT,2X,fd	—	—	—	23.7	25.5
60°,2X,sd	1.4/1.2	0.98	—	24.1	29
90°,2X,sd	—	—	1.1	23.2	32
RT,1/2X,fd	1.6/1.4	1.2	1.2	19.4	37
RT,1/3X,fd	1.8/1.6	1.4	1.4	16.9	45
RT,1/4X,fd	2.1/2.0	1.7	2.0	12.8	53
RT,1/6X,fd	2.9/2.5	2.2	2.2	9.3	126[g]
RT,1/8X,fd	—	—	—	10.4	124[g]
RT,1/10X,fd	—	—	2.4	6.2	144[g]
RT,1/12X,fd	—	—	2.6	11.9	163[g]

[a] Code for preparation conditions: (*a*,*b*,*c*), where *a* represents the temperature at which the reduction was carried out, *b* represents the RSH:$AuCl_4^-$ molar ratio before reduction, and *c* represents the rate of reductant addition (fd, 10 s; md, 2 m; sd, 15 m). [b] SAXS results for Au core radius determined from Guinier plot. [c] SAXS results from Porod plot. [d] HRTEM results, average Au core size from analysis of histogram of HRTEM images. [e] TGA for thermal loss of alkanethiolate fraction of clusters. [f] Proton NMR linewidths. [g] CH_3 ^{1}H NMR signal obscured; the CH_2 resonance was used instead for these clusters.

Nanoparticles - caracterization

TEM

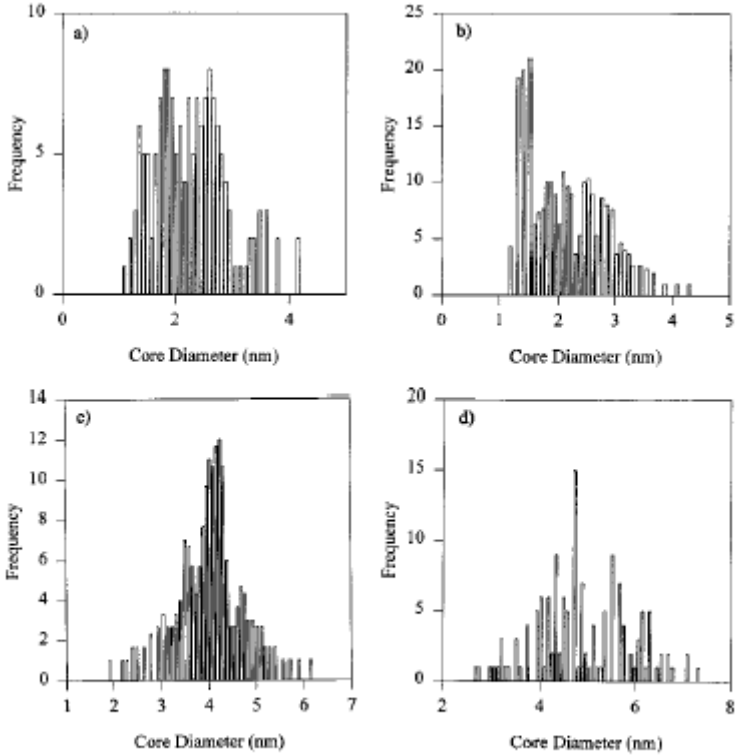

Figure 2. Size histograms (a and d are for films shown in Figure 1): (a) (0°,2X,fd); (b) (0°,2X,sd); (c) (RT,1/4X,fd); (d) (RT, 1/6X,fd).

NANOPARTICELLE - characterization

Table 2. Results from Modeling of Gold Core Sizes, Shapes, and Alkanethiolate Coverages, and of Size-Dependent T_2 Broadening of Proton NMR of CH_3 Resonances

#atoms (shape)[a]	R_{CORE}, nm	#surface atoms/ %defect/area nm^2	calc TGA %organic/ %coverage/#chains	calc R_{TOTAL}, nm	calc NMR ν_{FWHM}, Hz
79 (TO^+)	0.65	60/60%/8.30	33.0/63%/38	2.6	15
116 (TO^-)	0.71	78/61%/11.36	31.8/68%/53	2.6	16
140 (TO^+)	0.81	96/50%/11.43	27.9/55%/53	2.7	17
201 (TO)	0.87	128/47%/15.22	26.5/55%/71	2.8	18
225 (TO^+)	0.98	140/43%/15.19	24.4/51%/71	2.9	19
309 (CO)	1.1	162/52%/19.64	23.3/57%/92	3.0	22
314 (TO^+)	1.0	174/41%/19.46	22.9/52%/91	3.0	20
459 (TO^+)	1.2	234/36%/24.34	20.2/49%/114	3.1	23
586 (TO)	1.2	272/35%/28.94	19.1/50%/135	3.2	24
807 (TO^+)	1.4	348/31%/34.86	17.1/47%/163	3.3	27
976 (TO^-)	1.5	390/31%/40.02	16.4/48%/187	3.4	28
1289 (TO)	1.6	482/27%/47.22	14.9/46%/221	3.5	32
2406 (TO)	2.0	752/22%/69.86	12.2/43%/326	3.9	42
2951 (TO^+)	2.2	876/21%/79.44	11.4/42%/371	4.1	47; 94[b]
4033 (TO)	2.4	1082/19%/97.00	10.3/42%/453	4.3	55; 110[b]
4794 (TO^+)	2.6	1230/18%/108.28	9.7/41%/506	4.4	61; 122[b]
6266 (TO)	2.8	1472/16%/128.66	8.9/41%/601	4.7	70; 140[b]

[a] CO = cuboctahedron; TO = ideal truncoctahedron (all sides equal); TO^+ = truncoctahedron in which ($0 < n - m \leq 4$), where n is the number of atoms between (111) facets and m is the number of atoms between (111) and (100) facets; TO^- = truncoctahedron in which ($-4 \leq n - m < 0$, $m > 1$). [b] The second value is the calculated linewidth for the methylene peak.

NANOPARTICELLE - characterization

NMR

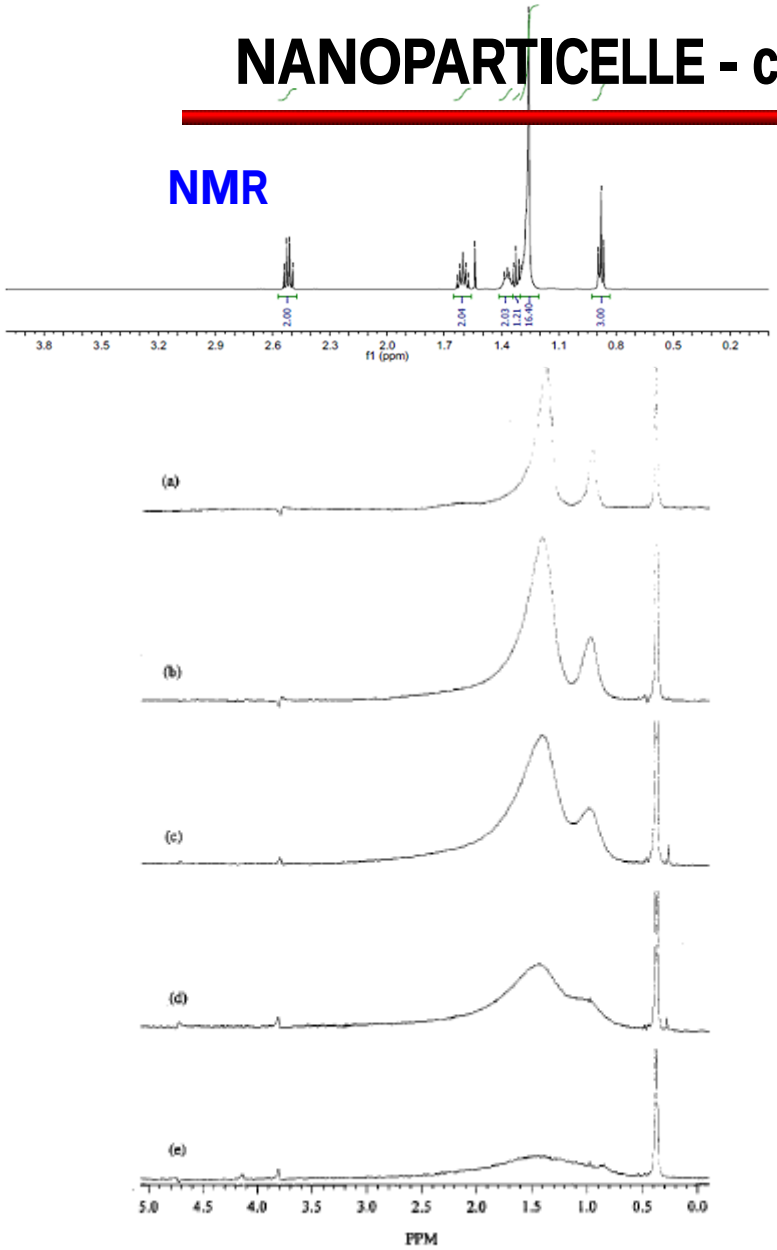

Figure 5. The ^{1}H NMR spectra (C_6D_6) of dodecanethiolate-protected Au clusters. Each spectrum was Fourier transformed using a line broadening of 1 Hz: (a) (−78°,2X,sd); (b) (90°,2X,sd); (c) (RT,1/3X,fd); (d) (RT,1/4X,fd); (e) (RT,1/12X,fd).

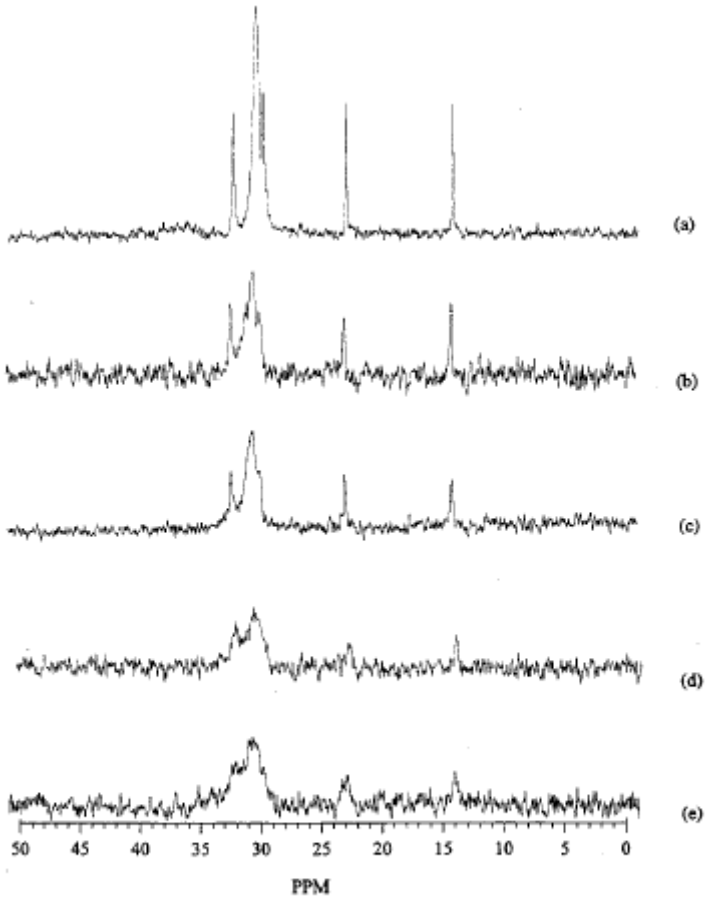

Figure 4. The ^{13}C NMR spectra (C_6D_6) of dodecanethiolate-protected Au clusters. Each spectrum was Fourier transformed using a line broadening of 3 Hz: (a) (−78°,2X,sd); (b) (90°,2X,sd); (c) (RT,1/3X,fd); (d) (RT,1/4X,fd); (e) (RT,1/6X,fd).

NANOPARTICELLE - characterization

UV-Vis

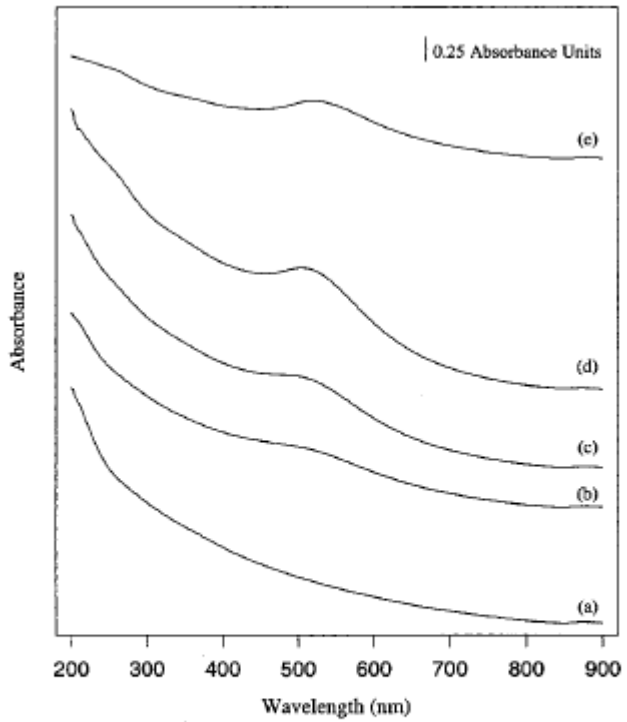

Figure 7. The UV/vis spectra (hexane) of dodecanethiolate-protected Au clusters: (a) (−78°,2X,sd), $C = 3 \times 10^{-6}$ M, MW $= 3.4 \times 10^4$ amu; (b) (90°,2X,sd), $C = 2 \times 10^{-6}$ M, MW $= 5.5 \times 10^4$ amu; (c) (RT,1/3X,fd), $C = 4 \times 10^{-7}$ M, MW $= 2.3 \times 10^5$ amu; (d) (RT,1/4X,fd), $C = 2 \times 10^{-7}$ M, MW $= 5.5 \times 10^5$ amu; (e) (RT,1/12X,fd), $C = 9 \times 10^{-8}$ M, MW $= 1.1 \times 10^6$ amu.

MPCC12

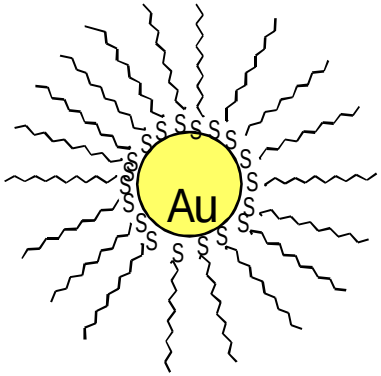

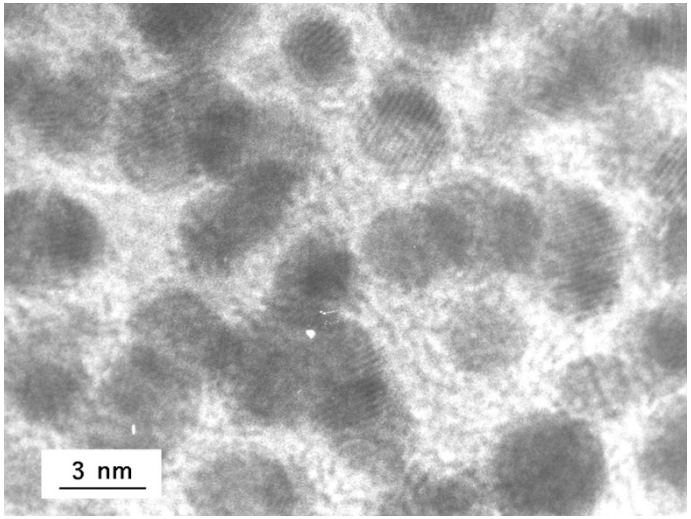

HRTEM

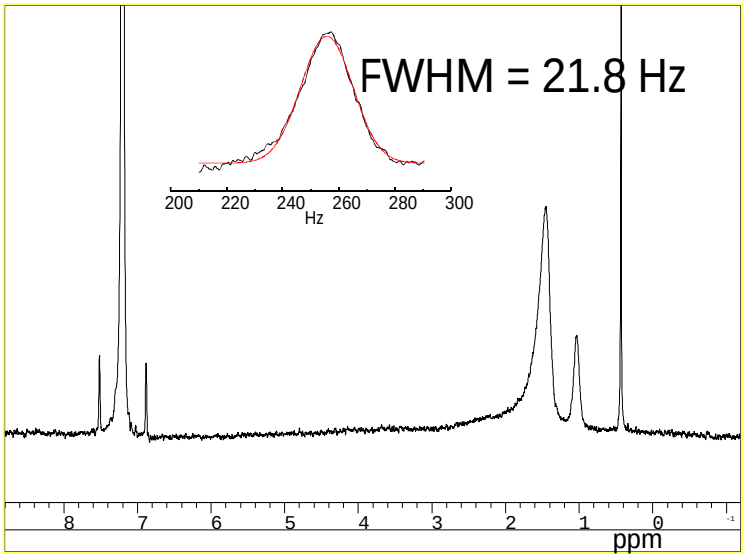

^{1}H NMR (250 MHz, C_6D_6)

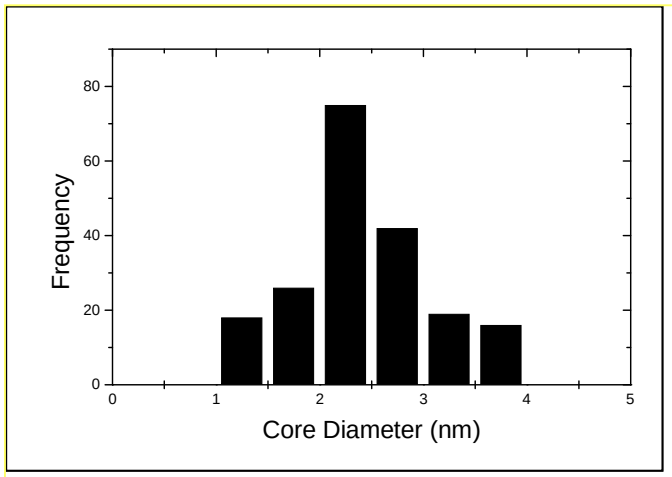

Core size histogram: core diameter 2.2 ± 0.4 n

MPC-C12

$Au_{116}(SR)_{50}$ (MW=)

MPC-C12 - TGA Analysis

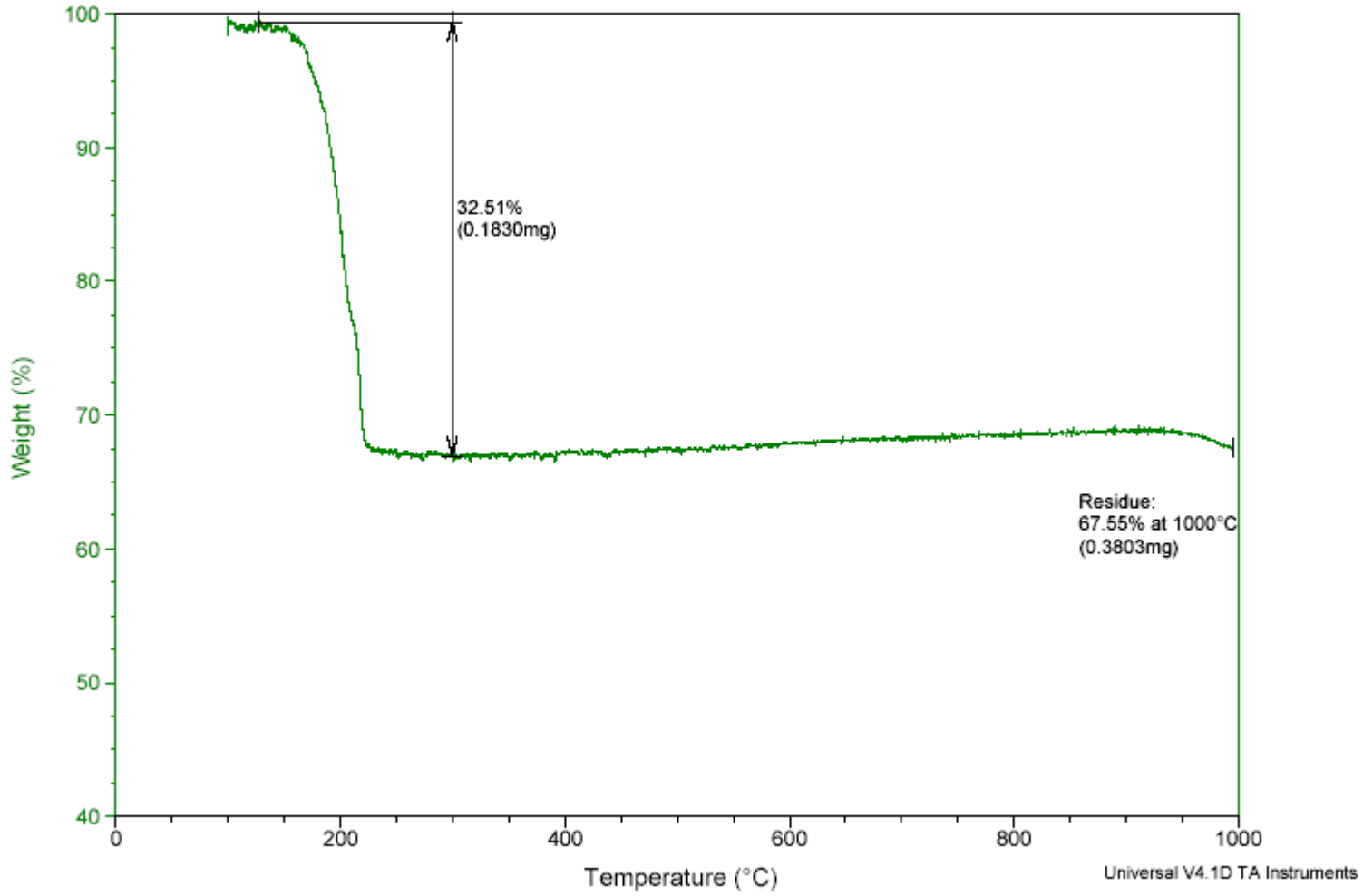

Water soluble nanoparticles

tiopronin

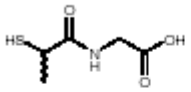

11

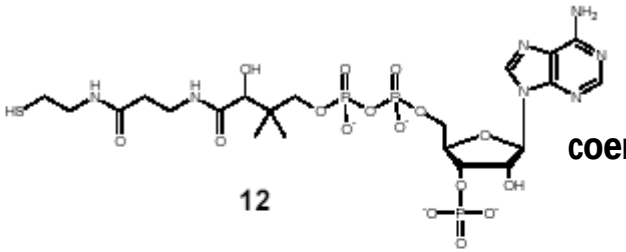

12

coenzyme A

13

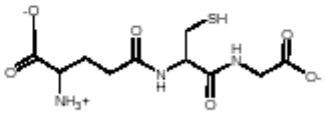

14 glutathione

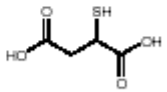

15

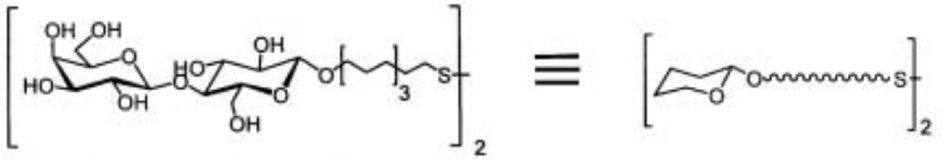

Lactose neoglycoconjugate

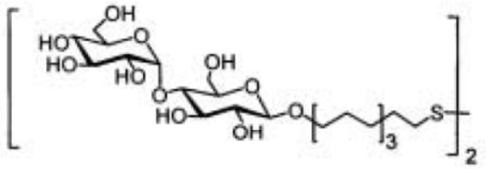

Maltose neoglycoconjugate

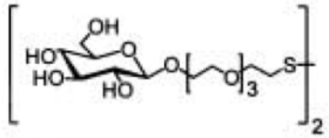

Glucose neoglycoconjugate

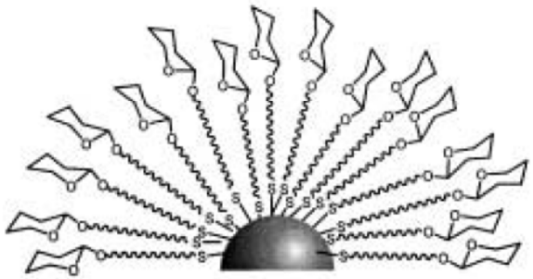

lacto-GNP
malto-GNP
gluco-GNP

Water soluble nanoparticles

$PEG_{5000}SH$

21

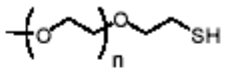

22a n = 1
22b n = 2
22c n = 3

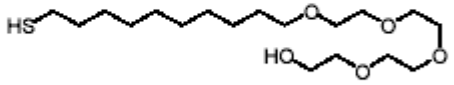

23

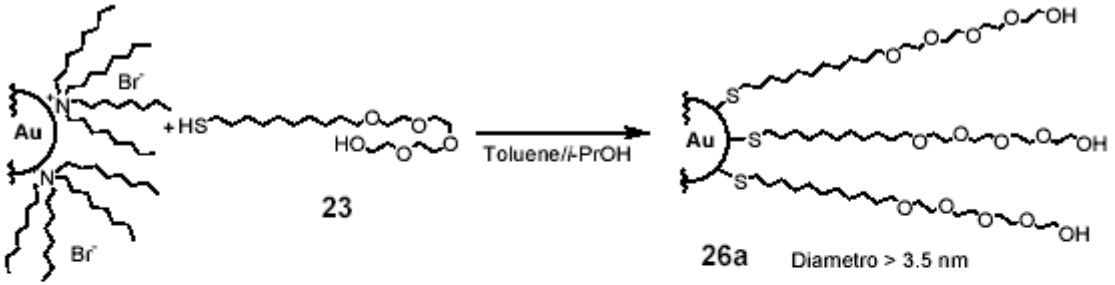

25

23

26a Diametro > 3.5 nm

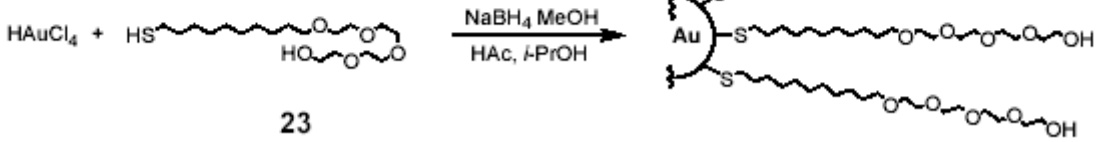

23

26b Diametro < 3.5 nm

Water soluble nanoparticles

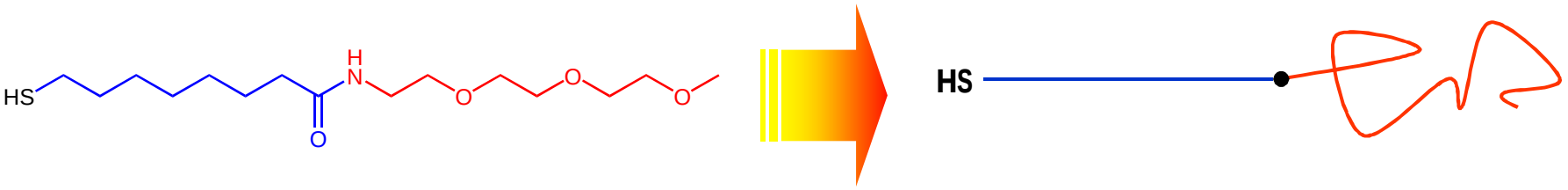

The hydrocarbon chain ensures the formation of a compact and tidy monolayer near the surface of the nanoparticle metal core

The polyether chain, even of short length, ensures MPCs solubility in water and polar solvents

$HAuCl_4$ + **HS** 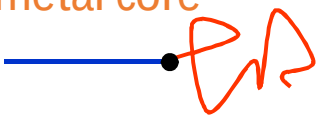 $\xrightarrow{MeOH/H_2O}$ $\xrightarrow{NaBH_4}$ Polyether-MPC

Homogeneous phase synthesis

Quantitative conversion of $HAuCl_4$

Diameter of the gold core 1.5 - 4.2 nm

Strong influence of the reduction rate

Pengo, P; Polizzi, S.; Battagliarin, M.; Pasquato, L.; Scrimin, P. J. Mater. Chem. **2003**, 13, 2471-2478.

MPC-C8-TEG Characterization

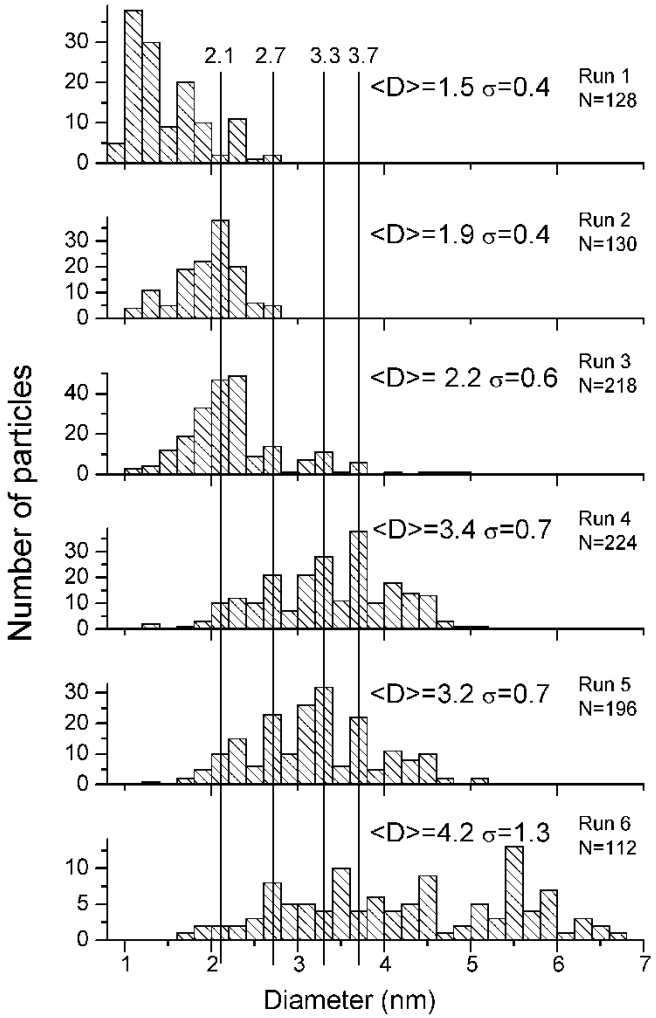

Increasing Gold / thiol ratio

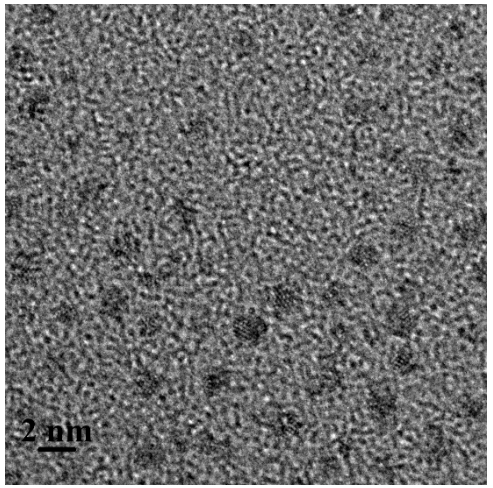

TEM image of MPCs obtained with a 1/3 gold/thiol molar ratio, $NaBH_4$ added in 10 sec.

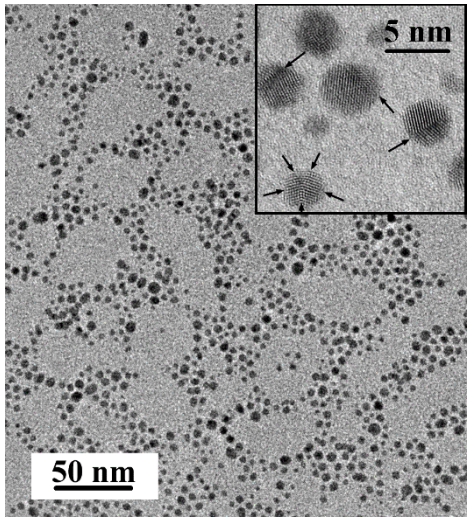

TEM image of MPCs obtained with a 3/1 gold/thiol molar ratio, adding $NaBH_4$ in 30 minutes

Thiolate Ligands for Synthesis of Water-Soluble Gold Clusters

C. J. Ackerson, P. D. Jadzinsky, R. D. Kornberg **J. AM. CHEM. SOC. 2005**, 127, 6550

Table 1. Water-Soluble Thiolates and Their Ability to Passivate Gold Clusters

compound name	published synthesis	diameter (nm)[k]	soluble product	stability	synthetic method[a]	behavior in HD–PAGE gel
3-mercaptopropionic acid	ref 21	undetermined[j]	yes	days to weeks	Brust	did not enter matrix in HD or LD−PAGE[i]
4-mercaptobutyric acid	no	4.0 ± 1.2	yes	weeks	Brust	not tested
3-mercapto-1,2-propanediol	ref 14[b]	4.7 ± 1.2	yes	days	Brust	single diffuse band in HD−PAGE
cysteine	ref 12[c]	1.6 ± 0.3	yes	days	Brust[f]	entered gel matrix as single band; stalled; single band in LD−PAGE
methionine	no	2.4 ± 1.0	yes	weeks	Hutchison	did not enter matrix in HD or LD−PAGE
thiomalate	ref 13[d]	2.1 ± 1.4	yes	weeks	Brust	single tight band surrounded by large halo
2-mercaptobenzoic acid	no	2.1 ± 0.9	yes	minutes	Brust	did not enter matrix in HD or LD−PAGE
3-mercaptobenzoic acid	no	1.6 ± 0.6	yes	days	Brust	did not enter matrix; single band in LD−PAGE
4-mercaptobenzoic acid	ref 7[e]	1.8 ± 0.4	yes	months	Brust	2 tight bands
tiopronin	ref 9	1.9 ± 0.7	yes	months	Brust[f]	single diffuse pink band in HD or LD−PAGE
selenomethionine	no	1.6 ± 0.4	yes	days	Hutchison	did not enter matrix in HD or LD−PAGE
1-thio-β-D-glucose	no	2.1 ± 0.5	yes[g]	months	Brust[f]	single band in LD−PAGE
glutathione	ref 8	1.4 ± 0.4	yes	months	Brust	5 bands
ITCAE pentapeptide[h]	no	1.4 ± 0.4	yes	days	Hutchison	not tested

[a] Brust synthesis was in 1:1 water:methanol with a 3:1 thiolate:gold ratio. Typical concentrations were 10 mM gold and 30 mM thiolate. A 5-fold molar excess of $NaBH_4$ in a volume of water ~10% of the reaction volume was added to complete the cluster formation. Reactions denoted Hutchison were performed as described (ref 5). [b] A 1:1 ratio of thiolate:Au(III) and a 9-fold BH_4^- excess. [c] Cystine was used as the starting material to create cysteine MPCs. [d] Highest organothiolate:Au(III) ratio used was 5:2, with equimolar $NaBH_4$ to $HAuCl_4$, likely resulting in incomplete reduction. [e] A 1.8:1 thiolate:Au(III) ratio was used. [f] These compounds failed to form soluble products in 1:1 water:methanol, but did so under similar conditions in 6:1 methanol:acetic acid. [g] This compound formed product that remained in suspension following low-speed centrifugation, indicating cluster formation, but failed to redissolve after methanol precipitation; this product was not repeatably precipitable in methanol, but could be purified from starting materials by gel filtration and, otherwise, behaved as a stable water-soluble MPC. [h] The pentapeptide had the sequence Ile-Thr-Cys-Ala-Glu. [i] LD−PAGE was a standard 12% SDS−PAGE gel. [j] Particles form aggregates within which individual particle diameters cannot be measured. [k] See Supporting Information for images, histograms, and further analysis.

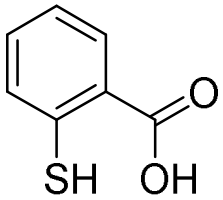

2-mercaptopropionic acid

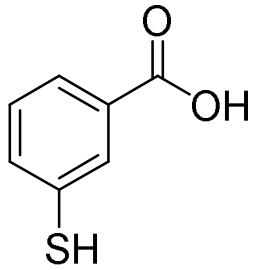

3-mercaptopropionic acid

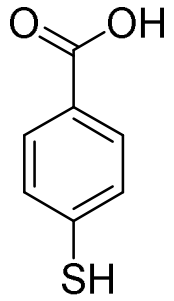

4-mercaptopropionic acid

Monolayer packing

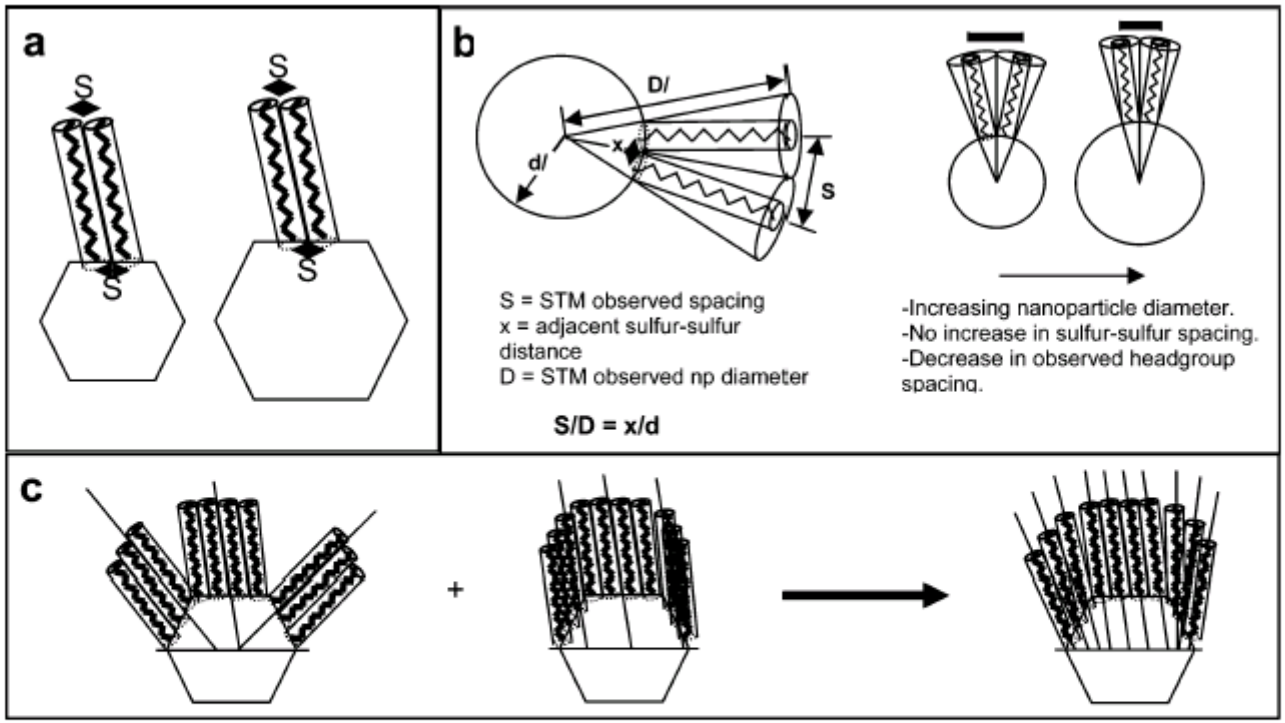

Figure 16. (a) Simplest representation of ligand packing for homoligand nanoparticles. Ligands pack on each nanoparticle facet as they would on a crystallographically equivalent flat 2-D gold surface, with a headgroup spacing corresponding exactly to the sulfur−sulfur spacing of the ligands at the nanoparticle core. (b) Schematic illustration of a ligand-coated nanoparticle relating the STM-observed headgroup spacing (S) at the periphery to the corresponding sulfur−sulfur spacing (x) at the nanoparticle core. (c) Ligands have essentially two configurations that they can assume on the faceted core: (i) they can assume their optimal tilt angle with regard to each facet (left), or (ii) they can assume a global tilt angle (middle). The first configuration leads to high-energy defects at the crystal edges, while the second does not take advantage of the particle curvature. Hence, the true configuration is likely a compromise between the two, with the ligands roughly conforming to a global tilt angle, but relaxing, and splaying outward as shown in the rightmost drawing in (c).

F. Stellacci et al. *J. AM. CHEM. SOC.* **2006**, *128*, 11135-11149.

Properties of the Monolayer

EPR Spectroscopy as a tool to investigate the monolayer properties

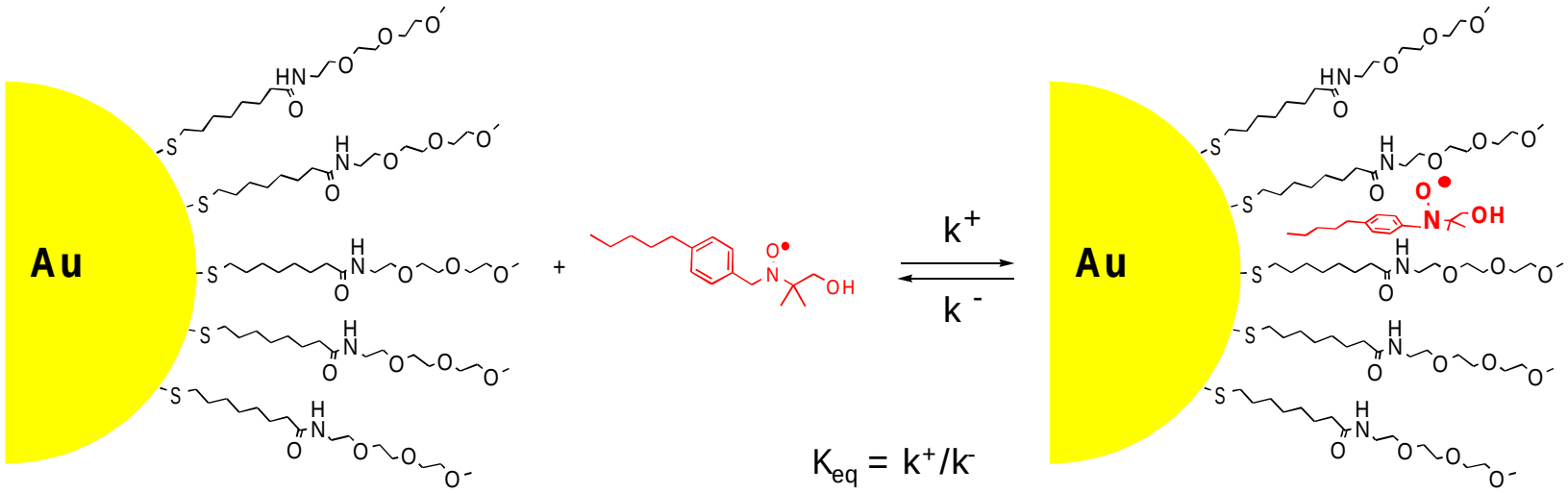

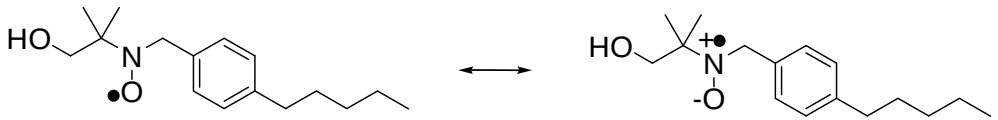

- the hyperfin coupling constants a(N) and $a(2H_\beta)$ are larger in polar media

M. Lucarini, P. Franchi, G. F. Peduli, P. Pengo, P. Scrimin, L. Pasquato, *J. Am. Chem. Soc.*, **2004**, *126*, 9326.

Properties of the Monolayer

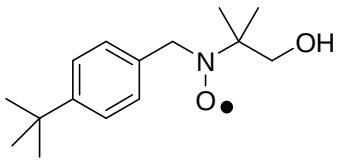

$1 \div 2 \times 10^{-5}$ M

k^+ $7.7\ 10^9\ M^{-1}s^{-1}$

k^- $1.9\ 10^6\ s^{-1}$

K_{eq} $5.683\ M^{-1}$

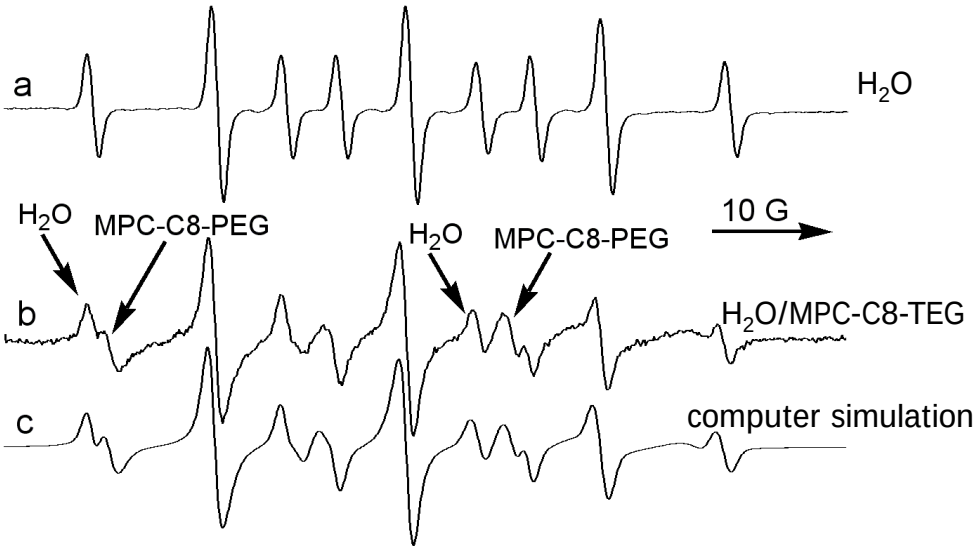

MPC-C8-TEG, d = 3.4 nm, σ 0.7 nm

- rapid exchange of the probe between the aqueous phase and the monolayer
- the nitroxide group is located in a less polar environment shielded from the aqueous solvent

M. Lucarini, P. Franchi, G. F. Peduli, P. Pengo, P. Scrimin, L. Pasquato, *J. Am. Chem. Soc.*, **2004**, *126*, 9326.

Monolayer packing

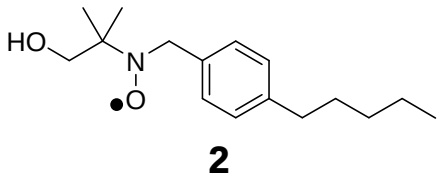

2

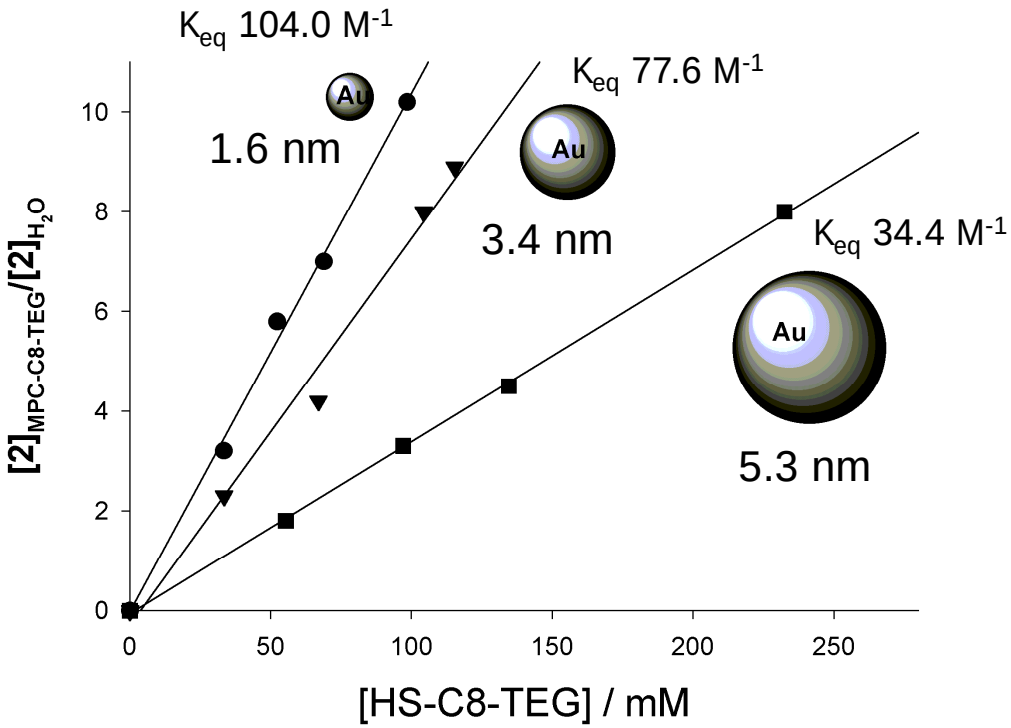

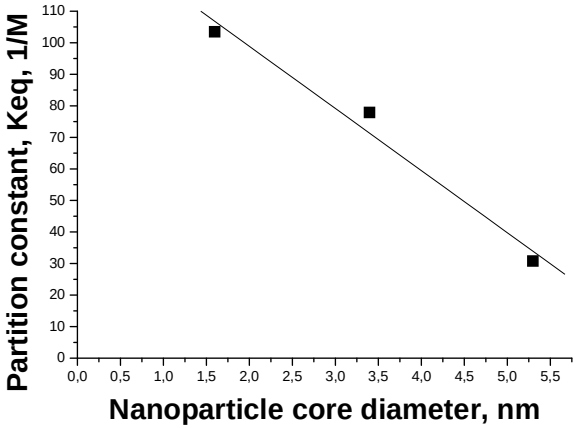

M. Lucarini, P. Franchi, G. F. Pedulli, C. Gentilini, S. Polizzi, P. Pengo, P. Scrimin, L. Pasquato, *J. Am. Chem. Soc.* **2005**, *127*, 16384.

Monolayer packing

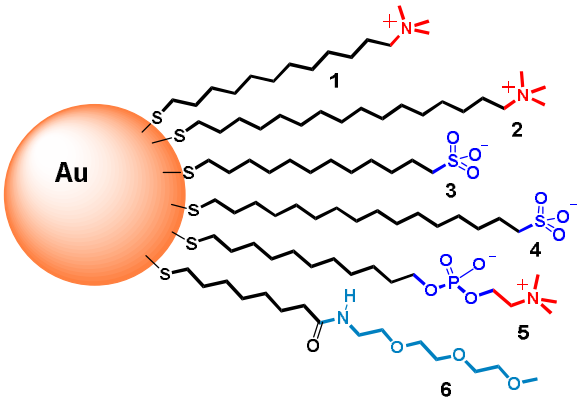

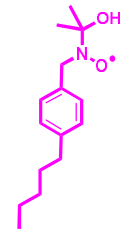

Table 1. Spectroscopic parameters for the radic equilibrium (K_{eq}) constants.

NP	T (K)	a_N (G)	a_{2H} (G)	K_{eq} (M^{-1})
-	300	16.25	10.14	
-	340	16.22	9.80	
NP-1	300	15.20	8.50	131
NP-1	340	15.35	8.46	20
NP-2	300	14.50[a]	8.45[a]	
		15.18	8.58	
NP-2	340	15.15	8.50	320
NP-3	300	15.15	8.40	133
NP-3	340	15.40	8.48	26
NP-4	300	14.40[a]	8.38[a]	
		15.23	8.30	
NP-4	330	14.58[a]	8.40[a]	
		15.33	8.33	
NP-4	340	15.32	8.40	98
NP-5	300	15.25	8.35	550
NP-6[b]	298	15.70	9.00	77

M. Lucarini, P. Posocco, L. Pasquato et al. manuscript in preparation 2020.

Monolayer packing

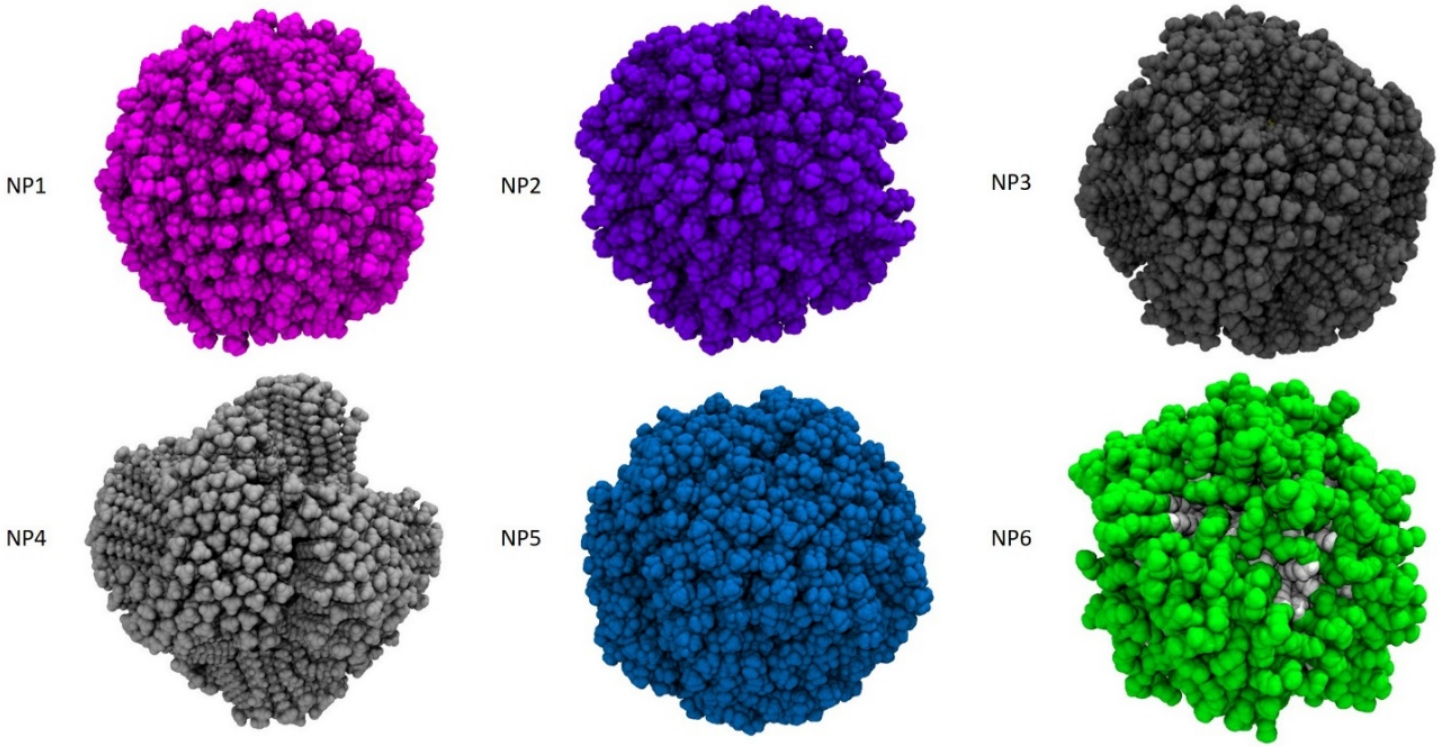

M. Lucarini, P. Posocco, L. Pasquato et al. manuscript in preparation 2020.

Monolayer packing

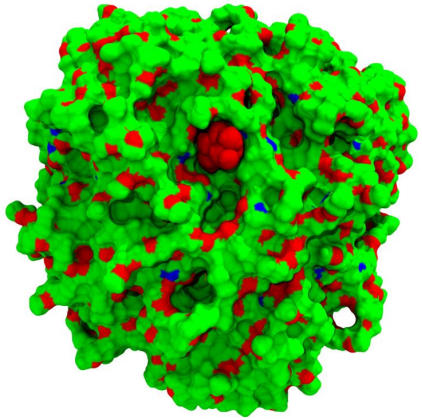

b)

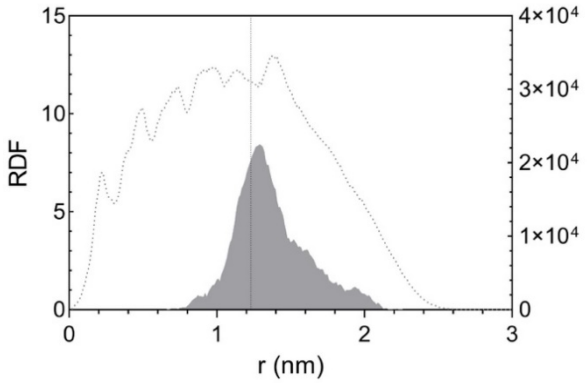

Figure S2. a) Binding of the radical probe (in red) within **NP6**. Solvent is omitted for clarity, oxygen atoms are in red and nitrogen atoms in blue, all the others atoms of the ligand are in green.
b) Radial distribution function (RDF) of nitrogen atom of the radical probe (solid line, left axis) and thiolate of **6** (dotted line, right axis) reported from the gold surface

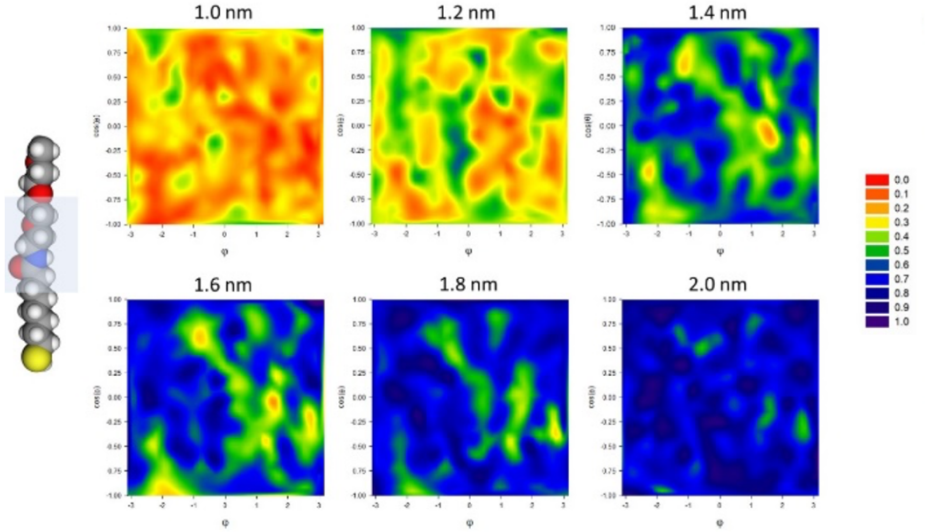

M. Lucarini, P. Posocco, L. Pasquato et al. manuscript in preparation 2020.

Monolayer packing

end group: ammonium ion solfonate

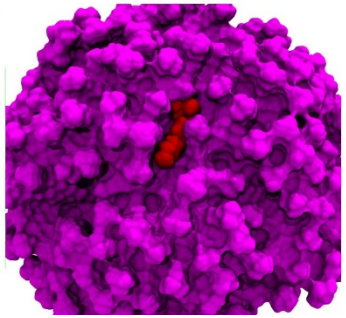

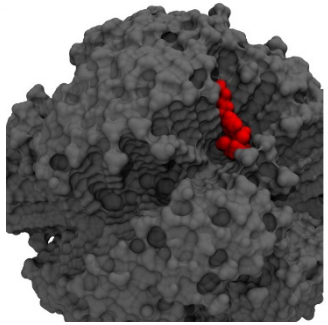

NP1 **NP3**

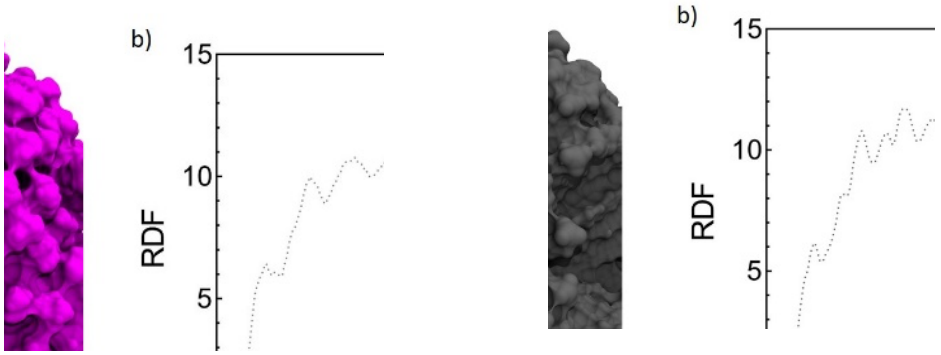

normalized water distribution at 1.2 nm from the gold surface

M. Lucarini, P. Posocco, L. Pasquato et al. manuscript submitted.

Monolayer packing

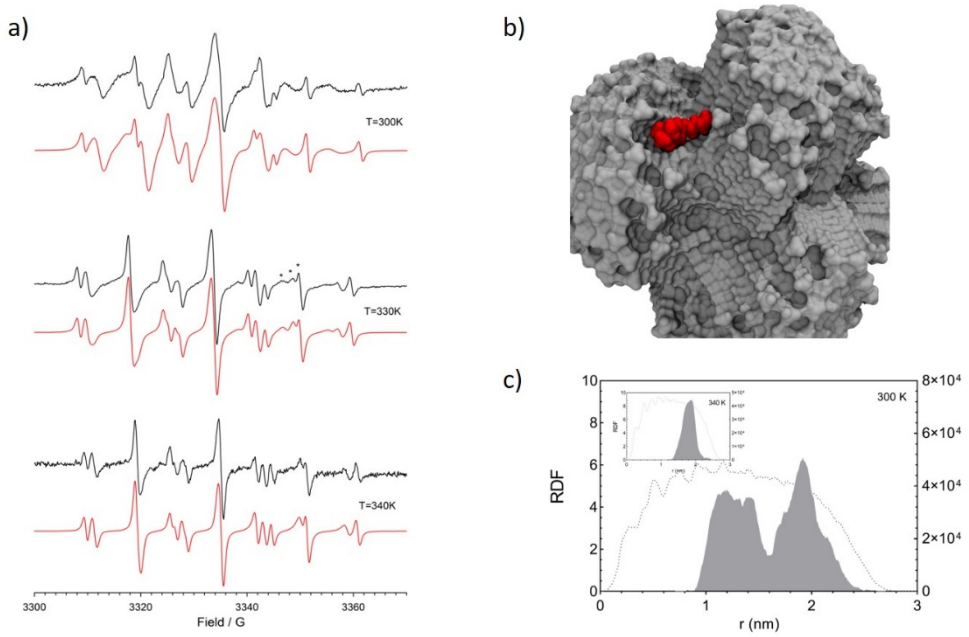

Figure 5. a) EPR spectra of the radical probe recorded in the presence of **NP4** (13.3 mg/0.1mL) at 300 K (top), 330 K (middle) and 340 K (bottom). Stars refer to the three different radical species (see text). In red are reported the corresponding theoretical simulations; b) Binding of the radical probe (in red) within **NP4**. Solvent is omitted for clarity. c) Radial distribution function (RDF) of nitrogen atom of the radical probe in the monolayer of **NP2** (solid line, left axis) and ligand **2** (dotted line, right axis) reported from the gold surface. Insert: same RDFs as in panel c), but predicted at 340 K.

M. Lucarini, P. Posocco, L. Pasquato et al. manuscript in preparation 2020.

Nanoparticles - functionalization

- **synthesis using a mixture of thiols**

  thiols should survive under the reaction conditions

- **Ligand exchange**

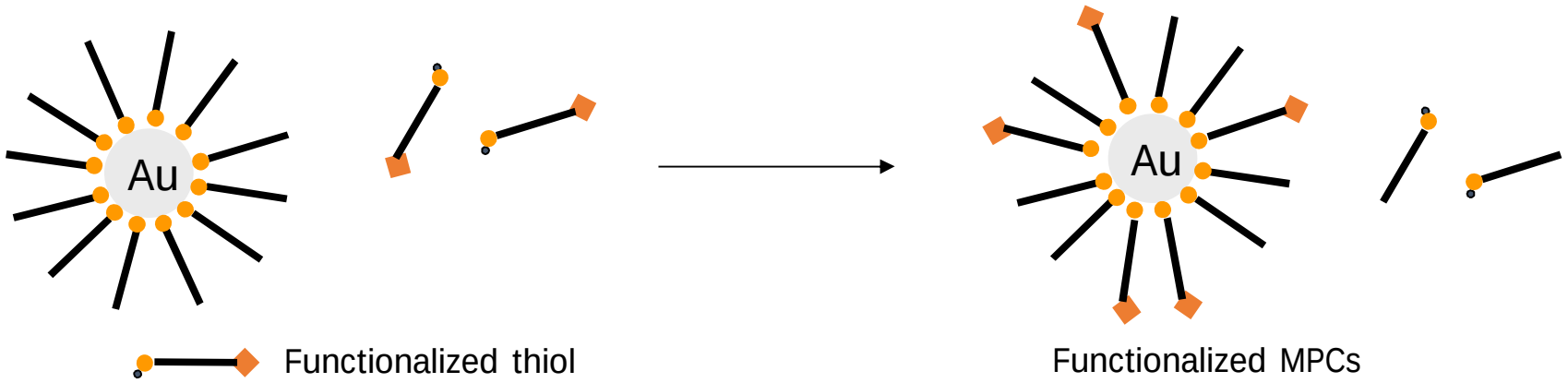

Hostetler, M. J.; Green, S. J.; Murray, R. W. J. Am. Chem. Soc., **1996**, 118, 4212 - 4213.

Nanoparticles - functionalization

Synthesis of the monolayer with a blend of thiols

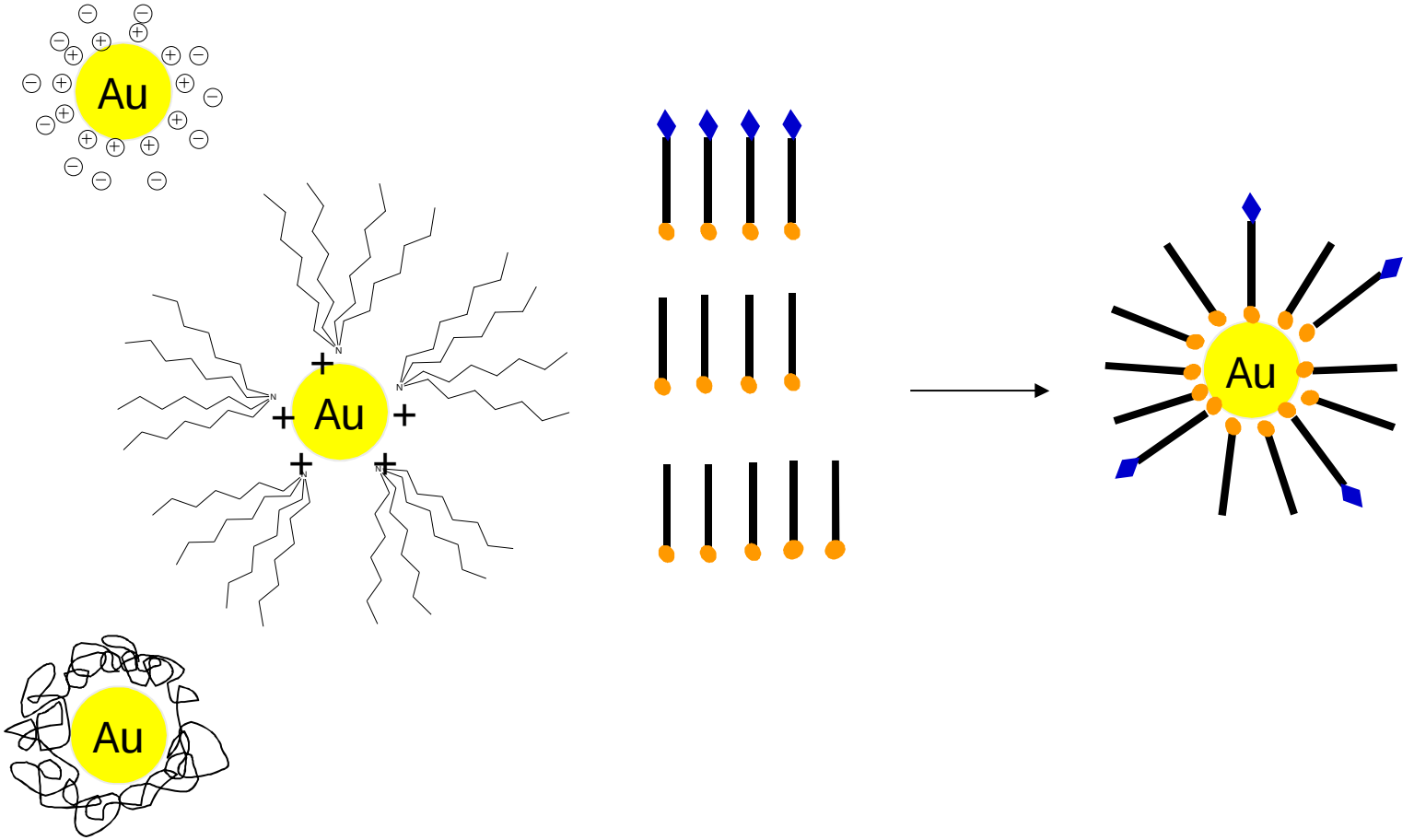

Nanoparticles - functionalization

Covalent Modification

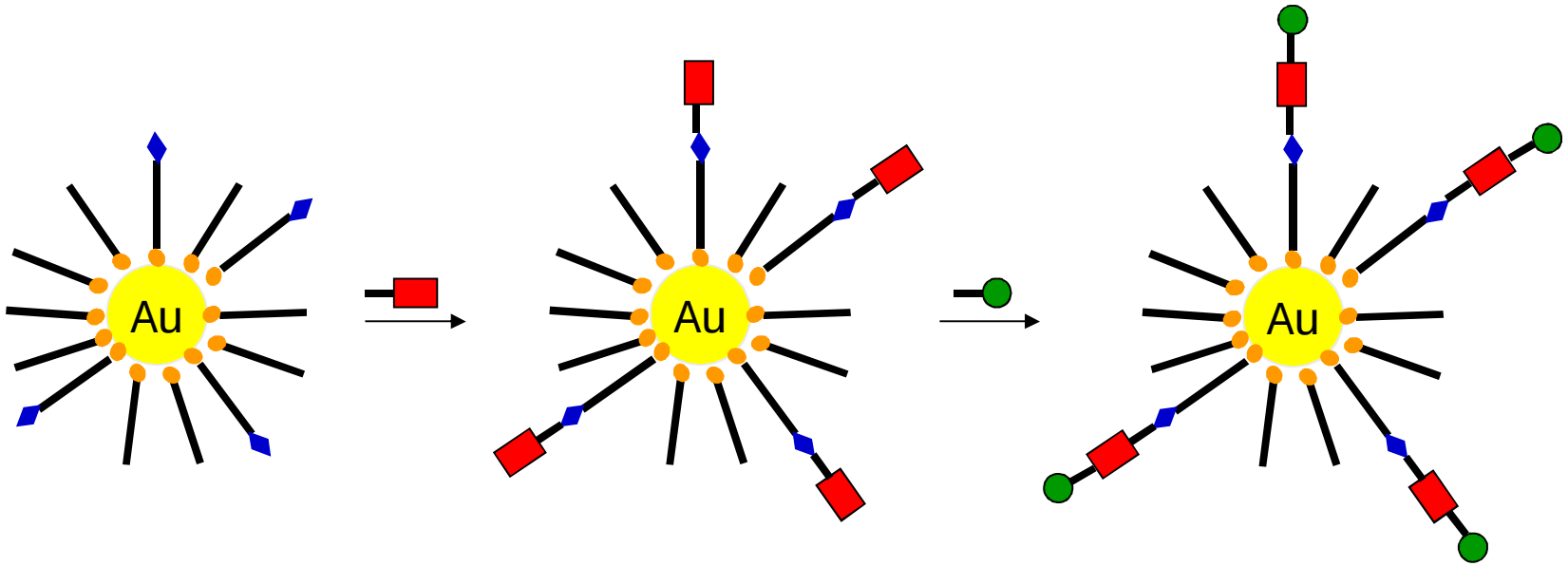

Templeton, A. C.; Hostetler, M. J.; Warmoth, E. K.; Chen, S.; Hartshorn, C. M.; Krishnamurthy, Murray, R. W. J. Am. Chem. Soc. **1998**, 120, 4845-4849.

Mixed Self-Assembled Monolayers

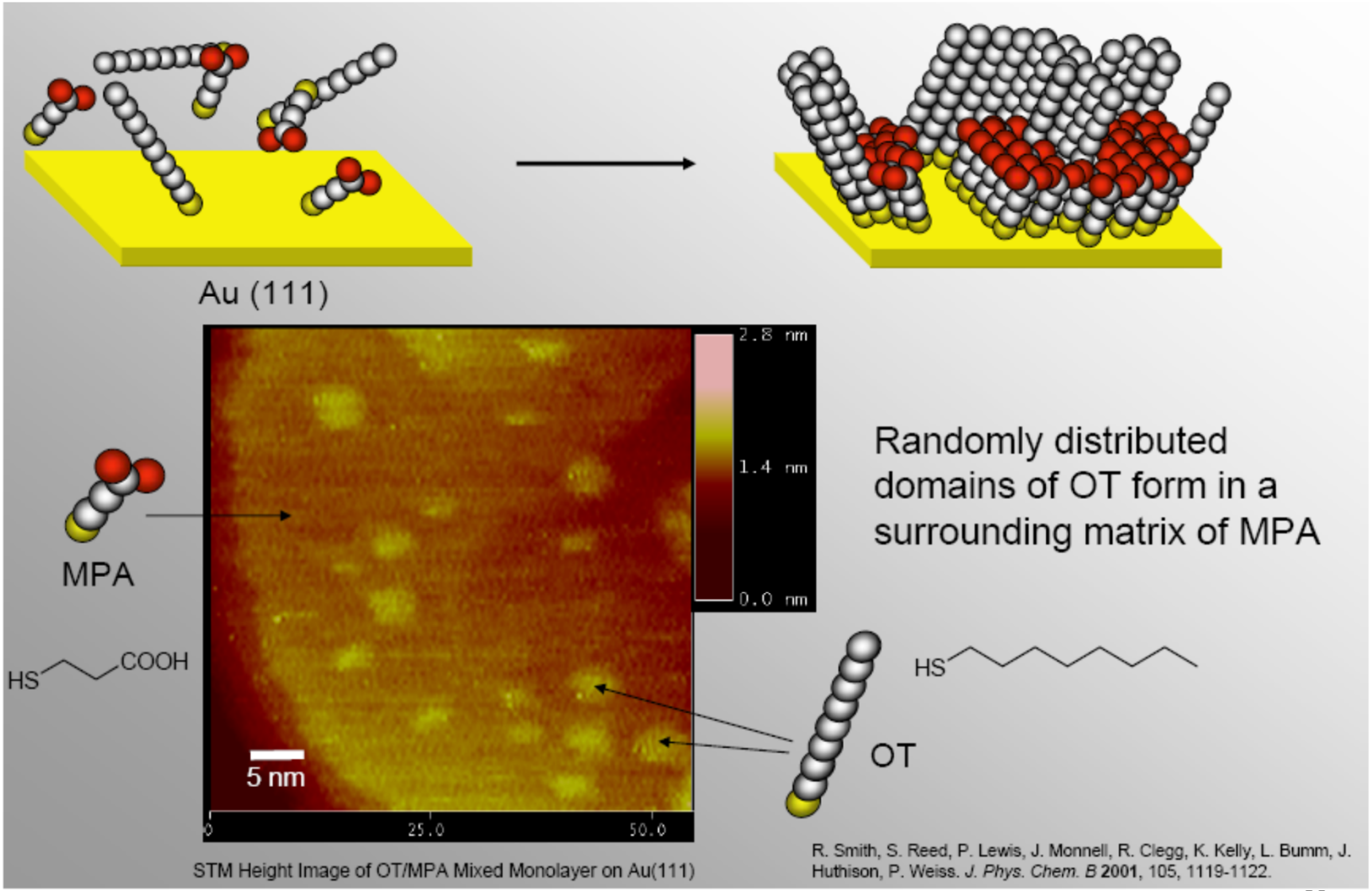

STM Height Image of OT/MPA Mixed Monolayer on Au(111)

R. Smith, S. Reed, P. Lewis, J. Monnell, R. Clegg, K. Kelly, L. Bumm, J. Huthison, P. Weiss. *J. Phys. Chem. B* **2001**, 105, 1119-1122.

Ordered Domains on NPs

Quantitative Analysis of Scanning Tunneling Microscopy Images of Mixed-Ligand-Functionalized Nanoparticles

Fabio Biscarini,*[,†] Quy Khac Ong,[‡] Cristiano Albonetti,[§] Fabiola Liscio,[∥] Maria Longobardi,[⊥] Kunal S. Mali,[#] Artur Ciesielski,[○] Javier Reguera,[‡] Christoph Renner,[⊥] Steven De Feyter,[#] Paolo Samorì,[○] and Francesco Stellacci[‡]

Langmuir 2013, 29, 13723−13734

topographical power spectral density (PSD)

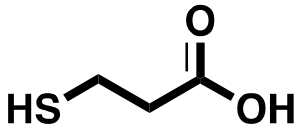

MPA

Octanethiol

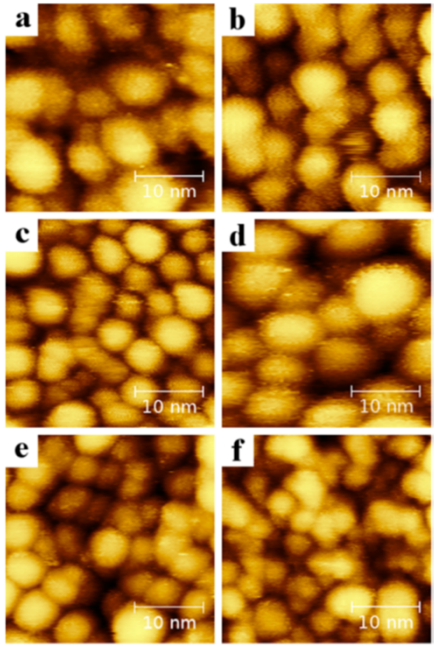

Jackson, A. M et al Nat. Mat., **2004**, 3, 330; Jackson, A. M. et al J. Am. Chem. Soc., **2006**

Determination of monolayer-protected gold nanoparticle ligand–shell morphology using NMR

Xiang Liu[1], Miao Yu[1], Hyewon Kim[2], Marta Mameli[1] & Francesco Stellacci[1]

Nature Commun. 2012

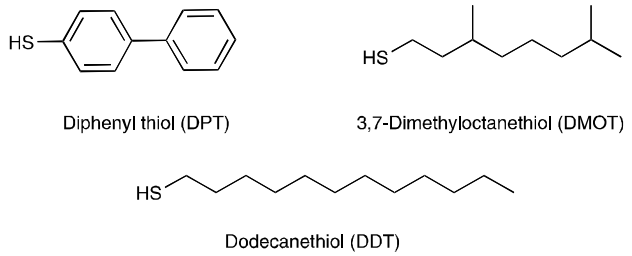

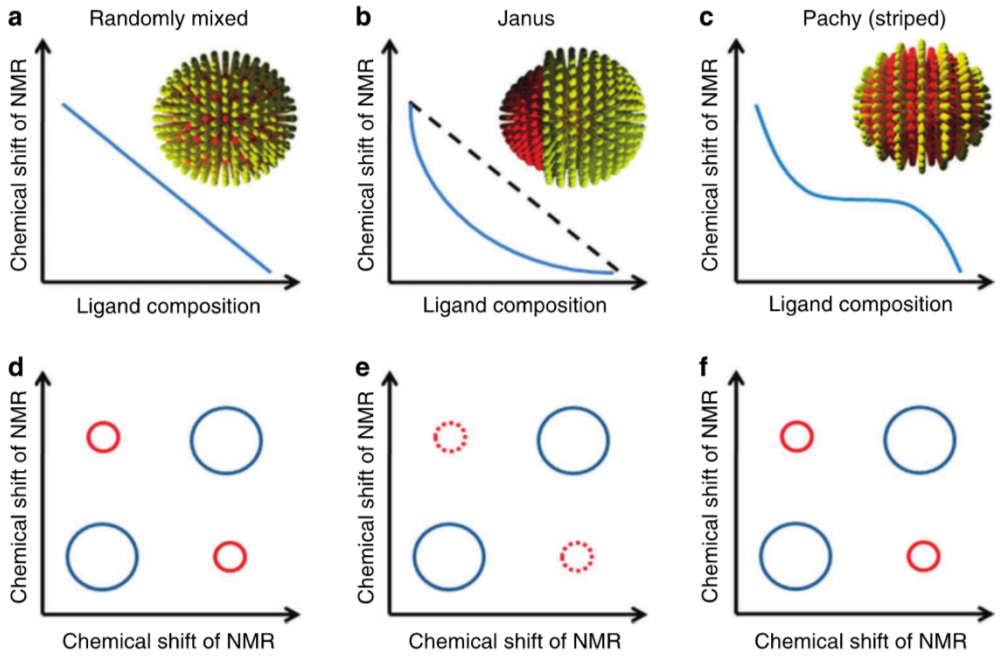

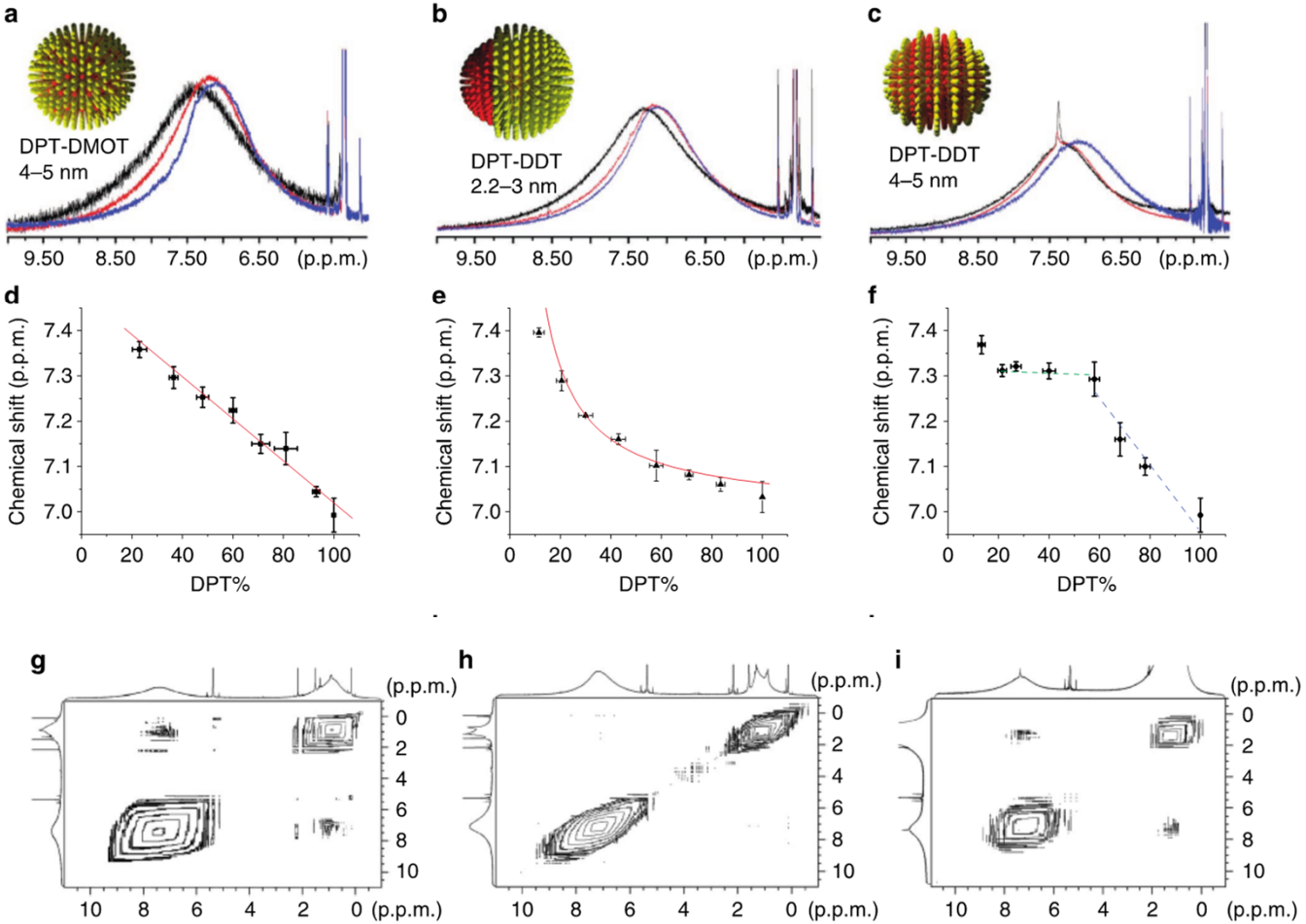
a
DPT-DMOT
4–5 nm
9.50 8.50 7.50 6.50 (p.p.m.)
b
DPT-DDT
2.2–3 nm
9.50 8.50 7.50 6.50 (p.p.m.)
c
DPT-DDT
4–5 nm
9.50 8.50 7.50 6.50 (p.p.m.)
d
Chemical shift (p.p.m.)
7.4 7.3 7.2 7.1 7.0
0 20 40 60 80 100
DPT%
e
Chemical shift (p.p.m.)
7.4 7.3 7.2 7.1 7.0
0 20 40 60 80 100
DPT%
f
Chemical shift (p.p.m.)
7.4 7.3 7.2 7.1 7.0
0 20 40 60 80 100
DPT%
g
(p.p.m.)
0 2 4 6 8 10
10 8 6 4 2 0 (p.p.m.)
h
(p.p.m.)
0 2 4 6 8 10
10 8 6 4 2 0 (p.p.m.)
i
(p.p.m.)
0 2 4 6 8 10
10 8 6 4 2 0 (p.p.m.)

Scanning tunneling microscopy and small angle neutron scattering study of mixed monolayer protected gold nanoparticles in organic solvents†

Mauro Moglianetti,‡[a] Quy Khac Ong,‡[a] Javier Reguera,‡[a] Kellen M. Harkness,[a] Marta Mameli,[a] Aurel Radulescu,[b] Joachim Kohlbrecher,[c] Corinne Jud,[d] Dmitri I. Svergun*[e] and Francesco Stellacci*[a]

Chem. Sci., 2014, **5**, 1232

Table 1 Contrasts of the phases in the hybrid particles (in units 10^{-6} $Å^{-2}$) (a) and discrepancy of the fits (b)

(a) Contrasts	C6 : d-C12	d-C6 : C12
Phase 1 : gold	1.4	1.4
Phase 2 : C12	2.5	−3.4
Phase 3 : C6	−3.4	1.9
(b) Discrepancy values[a]	**C6 : d-C12**	**d-C6 : C12**
Striped particle	1.2	1.1
Janus particle	15.2	7.7
Randomly mixed particles	1.8	4.2

[a] Chi squared.

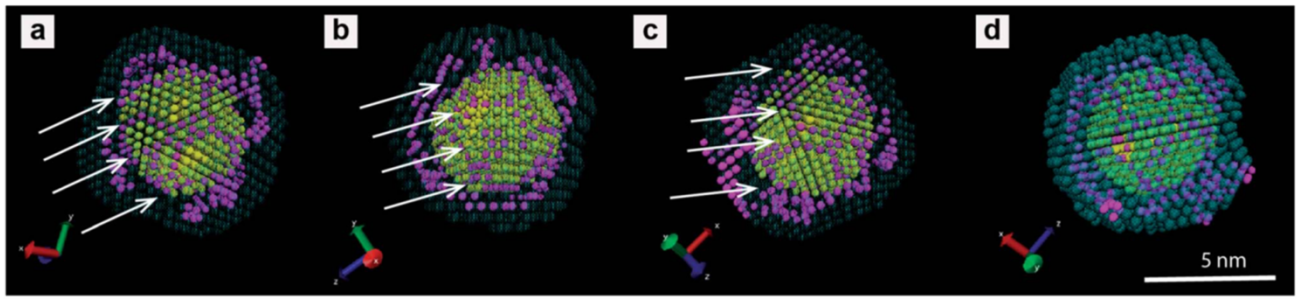

Fig. 5 Four different projections of a typical multiphase 3D low-resolution model of the C6 : C12 particles obtained from the fitting of the SANS data. Yellow beads indicate the gold nanoparticle core regions, the magenta beads represent the C6 moiety, and the cyan beads the C12 moiety. The beads in the model act as low-resolution place holders to depict the space occupied by the gold, C6 and C12 moieties. The image (d) on the right has the cyan beads in a lower transparency mode to highlight the C12 moieties. The C6 regions form elongated domains within the bulk of the C12 phase in excellent agreement with the model of striped nanoparticles. Scale bar, 5 nm. The arrows indicate elongated C6 domains that roughly align along a preferential direction. These features would provide aligned domain boundaries in the STM images (the arrows are spaced by about 1 nm).

Characterization of Ligand Shell for Mixed-Ligand Coated Gold Nanoparticles

Quy Ong,[†] Zhi Luo,[†] and Francesco Stellacci*

DOI: 10.1021/acs.accounts.7b00165
Acc. Chem. Res. 2017, 50, 1911−1919

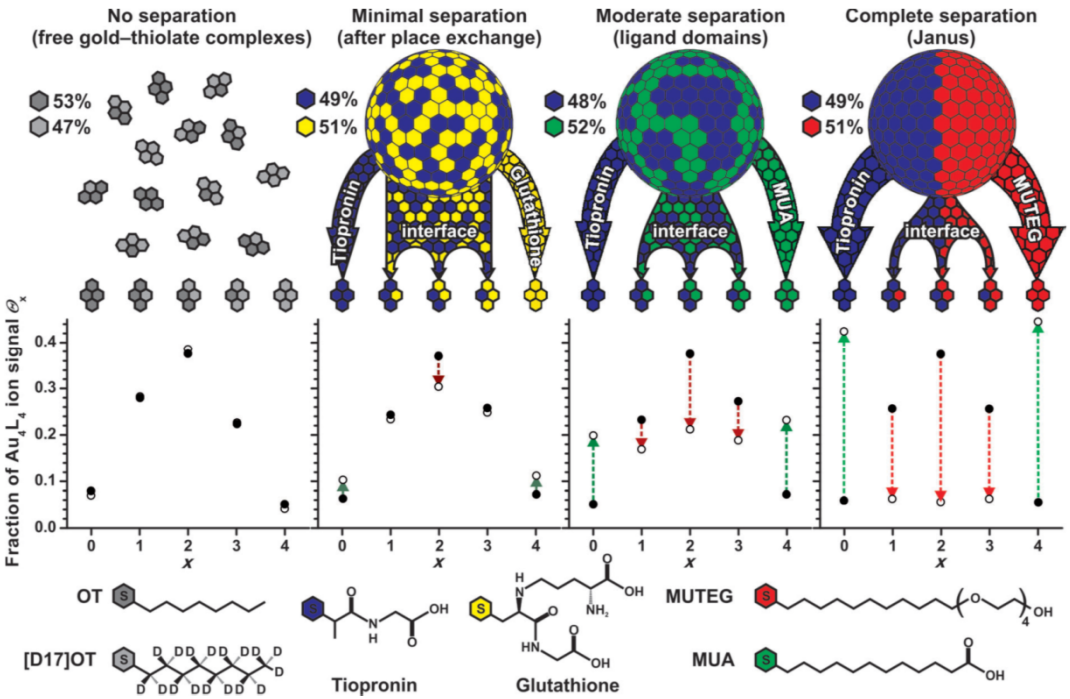

Figure 5. MALDI-MS investigation of molecular phase separation in mixed ligand coated NPs. Among the fragments of Au-thiol complexes caused by the MALDI process, only the Au_4L_4 ion species are analyzed since they are the most abundant fragments. For a binary ligand coated gold NP, 5 combinations of Au_4L_4 will be found and they are labeled from 0 to 4 in the x-axis of the plots. In other words, if the ligand shell contains a binary mixture of thiols A and B, the 5 species of the Au_4L_4 complexes analyzed are $Au_4A_{4-x}B_x$ (x = 0, 1, 2, 3, 4). Their corresponding abundances obtained experimentally from 4 different types of mixed ligand coated gold NPs are illustrated by open circles. The binomial distribution, which corresponds to random morphology, is presented by filled black dots. The deviations from the binomial distribution, represented by an arrow for each species, indicate the presence of molecular phase separation in the ligand shell that ranges from completely mixed, to patchy domains, and to the Janus structure. The ligand shell compositions of the 4 investigated particles are octanethiol (OT)/deuterated OT, tiopronin/glutathione, 11-mercaptoundecanoic (MUA)/glutathione, tiopronin/mercaptoundecyltetraethylene glycol (MUTEG), respectively. Reproduced with permission from ref 35. Copyright 2011 Wiley-VCH.

Entropy-Mediated Patterning of Surfactant-Coated Nanoparticles and Surfaces

Chetana Singh,[1] Pradip K. Ghorai,[1] Mark A. Horsch,[1] Alicia M. Jackson,[2] Ronald G. Larson,[1]
Francesco Stellacci,[2] and Sharon C. Glotzer[1,3,*]

PRL 99, 226106 (2007)

AuNP 7.0 nm in diameter

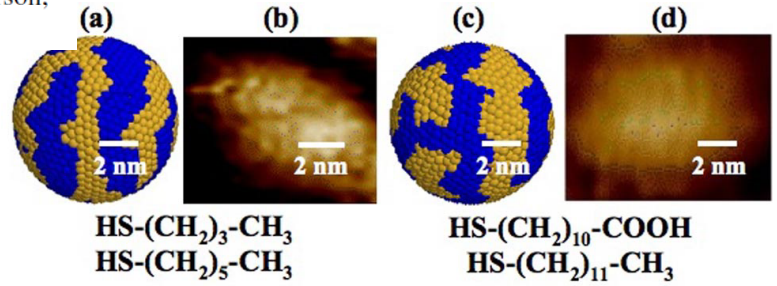

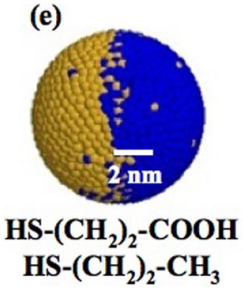

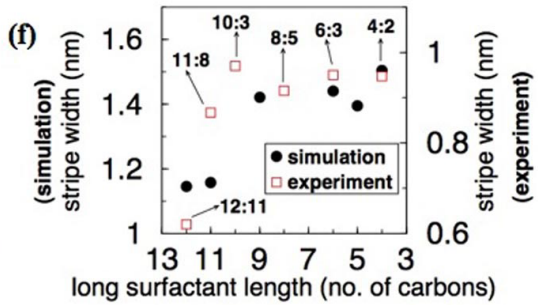

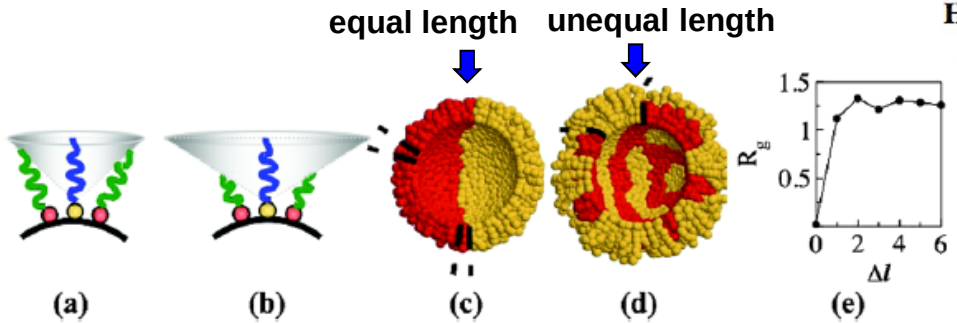

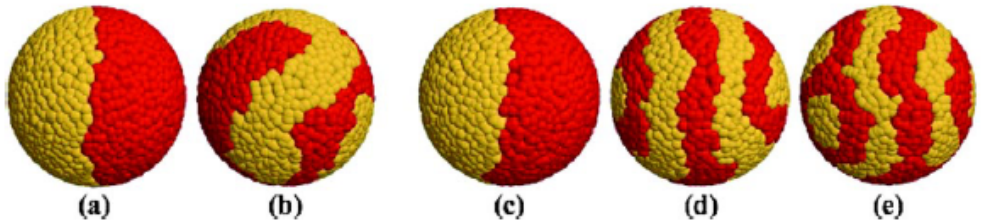

(a) Length ratio 4:4, equal bulkiness. (b) Length ratio 6:6 with one surfactant (yellow heads) having a bulkier tail group. (c)–(e) Length ratios 4:6, 4:7 and 4:13, respectively, with equal bulkiness.

morphologies of mixed-monolayers

Entropy-Mediated Patterning of Surfactant-Coated Nanoparticles and Surfaces

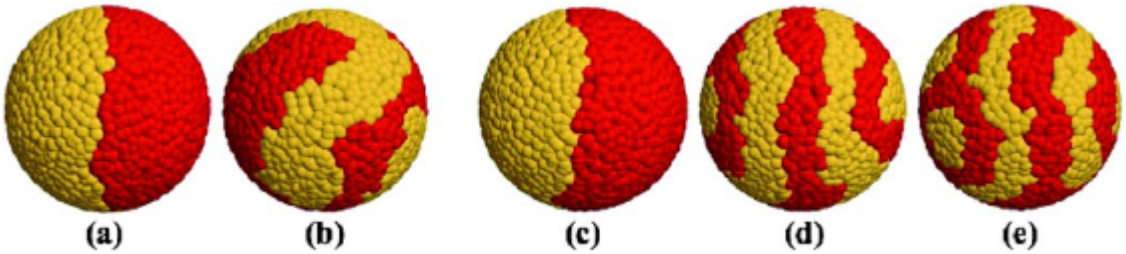

same length

same length different tail group bulkiness

4:6

4:7

4:13

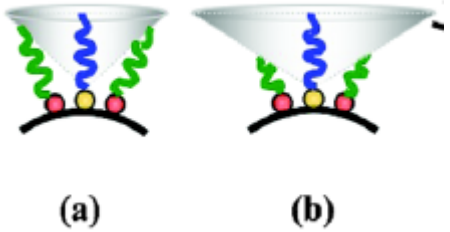

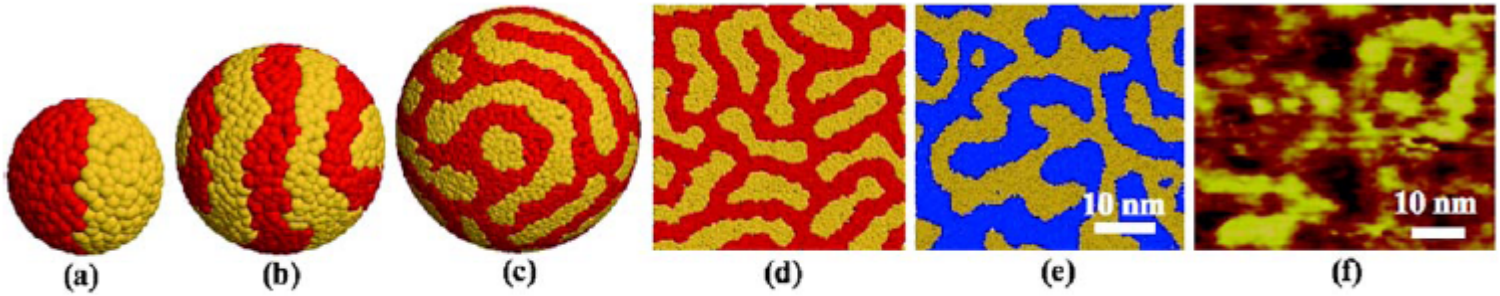

surfaces with varying degrees of curvature, different length C4:C6, same end group.

mixed-monolayer properties

tuning the surface chemistry

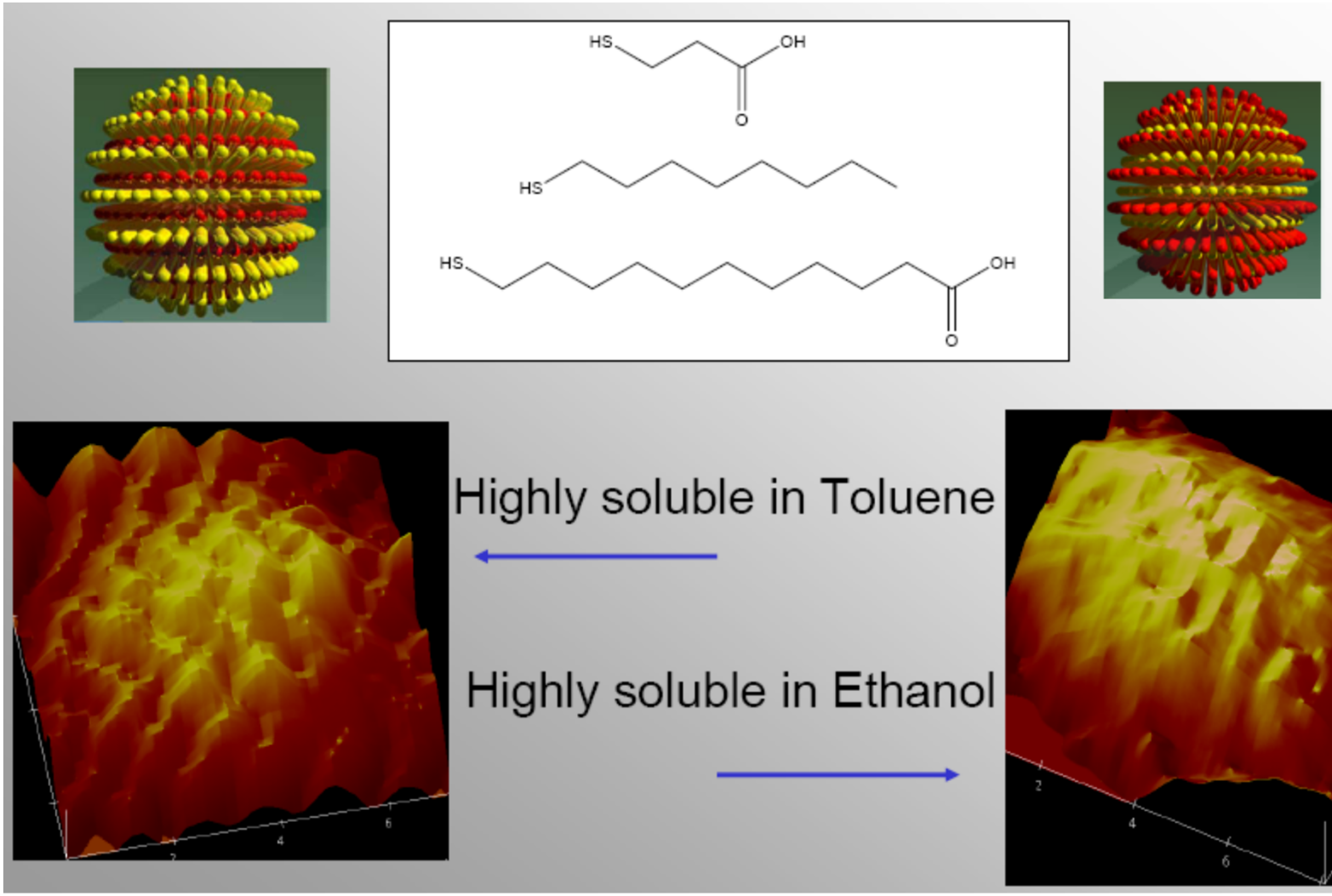

Centrone, A. et al PNAS, **2008**, 105, 9886.

mixed-monolayer properties

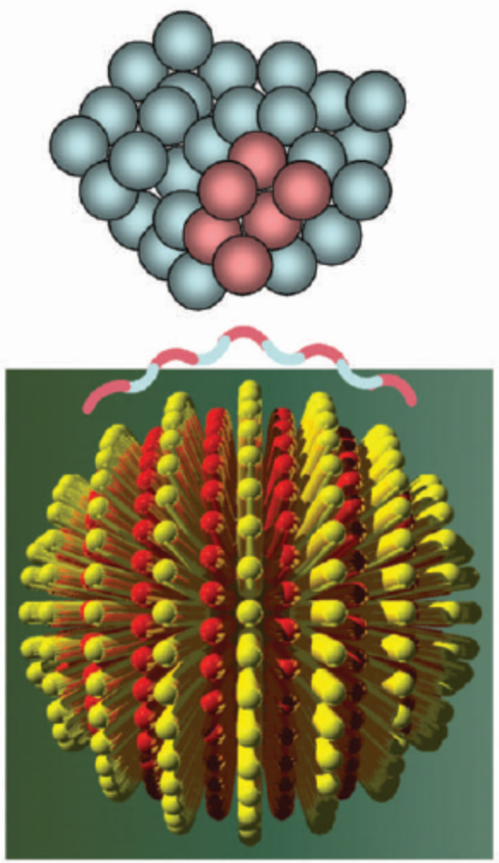

Figure 5 Schematic drawing of a generic protein (top) and a rippled nanoparticle (bottom). The pink and blue contour line on top of the nanoparticle shows the hydrophobic and the hydrophilic regions of the particle,respectively.The same colour scheme is used to show the outside shell of the chosen protein.It is evident (as the drawing is approximately to scale) how,despite the enormous conformational freedom that the proteins

A. M. Jackson, J. W. Myerson, F. Stellacci, Nat. Mater. **2004**, 3, 330-336.

protein nonspecific absorption

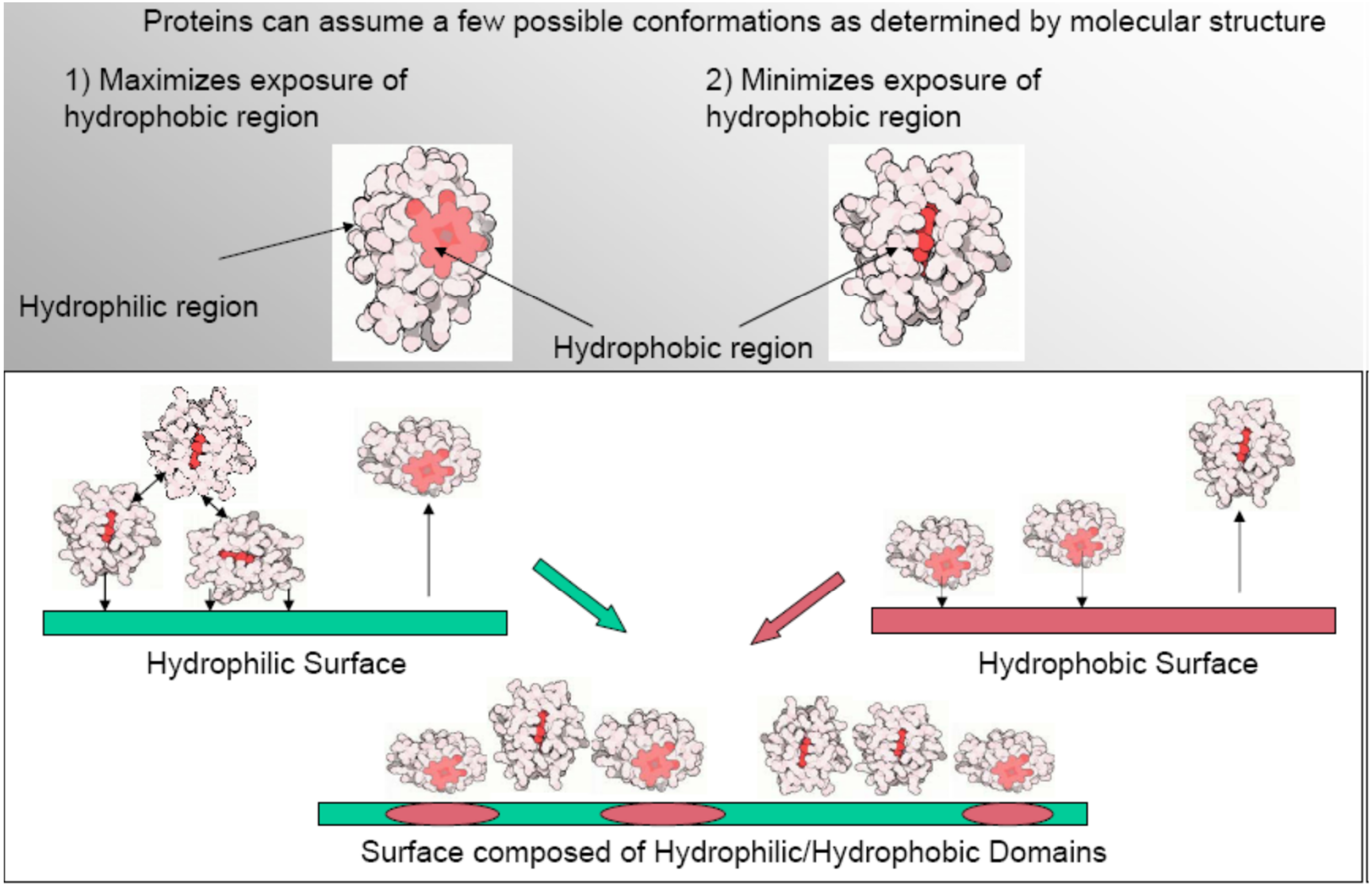

The Nano Lotus Leaf Effect

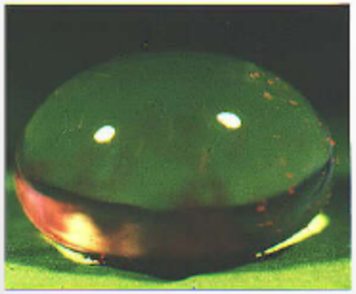

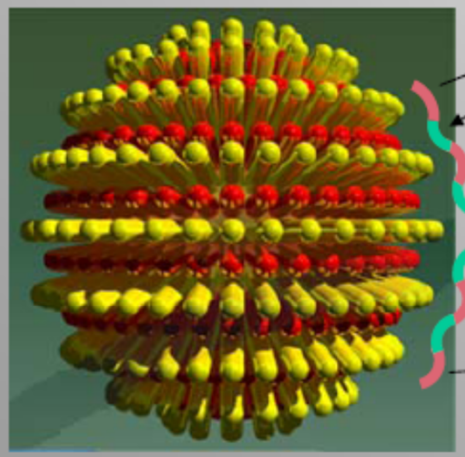

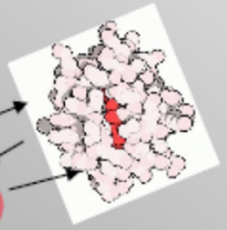

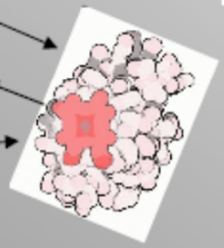

Size of hydrophobic/hydrophilic regions of protein are greater than size scale of ligand domains on the nanoparticles.

Proteins are conformationally frustrated and cannot adsorb to nanoparticle surface.